MUTUAL PHASE-CONJUGATION SCHEME FOR FIBER-NONLINEARITY MITIGATION IN COHERENT OPTICAL COMMUNICATION SYSTEMS

A DISSERTATION
SUBMITTED TO THE DEPARTMENT OF ELECTRICAL ENGINEERING
AND THE COMMITTEE ON GRADUATE STUDIES
OF THE UNIVERSITY of TOKYO
IN PARTIAL FULFILLMENT OF THE REQUIREMENTS
FOR THE DEGREE OF
MASTER OF SCIENCE

Hongbo Lu
August 2013

Preface

For the proposal of next generation of optical network over 100G, the fiber-nonlinearity distortion is the major obstacle. Three proposals have been extensively explored. The proposal of using high order modulation format requires high signal-to-noise ratio, which inevitably intensifies the fiber nonlinearity. The proposal of superchannel utilizes ultra-wide spectrum to increase the transmission speed of a single channel. The fiber nonlinearity becomes severer as well because of the use of the wider spectrum. For the multi-mode scheme, the severe fiber nonlinearity stemmed from mode-coupling is the major issue.

To tackle the issue of fiber-nonlinearity, there have been extensive research works explored. The back-propagation method has been recognized as the most promising one for its high performance to mitigation the fiber-nonlinearity distortion. However, the implementation of such method is not feasible for real-time system.

This thesis demonstrates a promising technique to solve the issue of fiber nonlinearity with high performance and feasibility for real-time system implementation for coherent optical fiber communication system. Such a system can be realized in a polarization-diversity scheme by transmitting two mutually phase-conjugated signals. We call this scheme the *mutual phase-conjugation* scheme. It provides 3-dB intrinsic nonlinear power tolerance improvement. Furthermore, the self-phase modulation distortion can be removed effectively by pre-dispersion on the mutually phase-conjugated signal. We call the method the *parallel back-propagation* method. These two methods provide a different approach to tackle the fiber-nonlinearity problem.

Acknowledgement

I would like to offer my greatest gratitude to my supervisor, Professor Kazuro Kikuchi, for the continuous supports, infinite patience and insightful advice. I am very grateful to him for all his time to tutor my study and guide my research.

I would like to acknowledge the Ph.D students and graduates in Kikuchi Lab, Mori Yojiro and Chao Zhang, for their help and discussion of the research topics. I would like to acknowledge Prof. Ozeki for his help and discussion in understanding the principle of parallel back-propagation method. I would like to acknowledge Assistant Professor Koji Igarashi (currently KDDI labs) for his fruitful discussion for the research proposals and the tutoring for the experiments. I also want to thank all the lab members, Han Changyo, Daiki Hiraoka, Yuki Yoshimura and Shota Ishimura for the fruitful discussion. I appreciate the academic assistance from Mr. Kazuhiro Katoh and Ms. Baba.

At last, I would like to thank my parents for all the supporting and understanding, for my life and for my research.

Contents

List of Figures

Chapter 1

Introduction

In this chapter, we introduce the background of this thesis. The history is reviewed to provide an abstractive understanding of the research trend in optical fiber communication. Proposals for the next generation optical networks over 100G are discussed, along with the major obstacles for the realization of the optical networks over 100G. The contributions of this thesis are summarized in this chapter − the mutual phase-conjugation method and the parallel back-propagation method for fiber-nonlinearity mitigation. Finally it's the organization of this work.

1.1 General background

1.1.1 History of optical fiber communication

The optical fiber communication is constructed by two key components: the laser and the silicon fiber. The invention of laser [1] enables the signal to be transmitted on lightwave, which allows the use of ultra-wide range spectrum window. Second, the groundbreaking work of optical fiber [2] creates a suitable waveguide for lightwave propagation. The modulated light is able to be transmitted with low energy loss [3, 4]. The optical fiber distinguishes with other communication manners in two elements: loss energy loss and ultra-wide spectrum window.

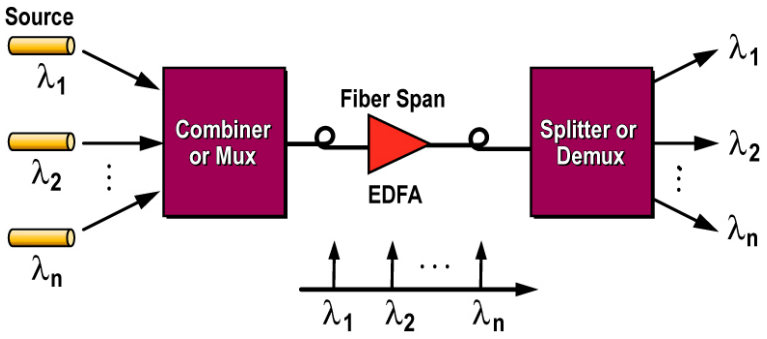

Figure 1.1: Schematic diagram for WDM optical system

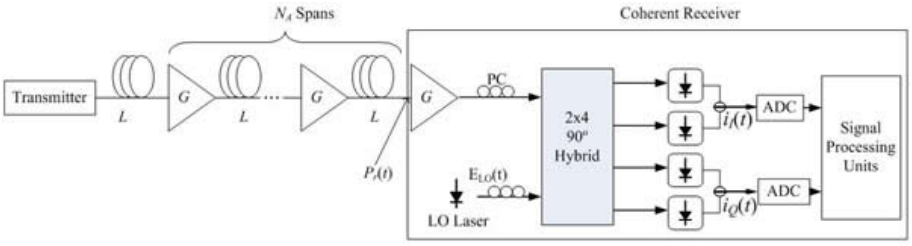

Figure 1.2: Configuration of conventional digital coherent fiber system

After decades of evolution in optical fiber communication, the optical network becomes the cornerstone for the physical structure of Internet. In the state-of-art 100G optical network, two techniques construct the fundamental frame: the wavelength-division multiplexing (WDM) system and the digital coherent receiver.

The WDM system significantly improves the fiber capacity up to a hundred times by simultaneously transmitting a bunch of modulated signals on different wavelengths within one single fiber [5, 6, 7]. The system diagram is shown in Fig. 1.1. In stead of limited by the speed of modulator, the available spectrum window is extended to the wavelength range of the optical amplifier installed in the fiber system. Furthermore, thanks to the invention of Erbium Doped Fiber Amplifier (EDFA) [8, 9], attenuated optical signals on different wavelength are compensated for simultaneously. The commercial EFDA offers C band wavelength window (1530 nm to 1565 nm), equivalent to over 4 THz frequency window.

The digital coherent receiver revolutionized the the design of fiber system [10, 11]. A schematic diagram of coherent optical system is shown in Fig. 1.2. With the introduction of the digital coherent receiver, the concept of spectrum efficiency (SE) is adopted with the use of multi-level modulation format [12, 13, 14]. The digital coherent receiver can detect the full information of the incident lightwave and converts it into digital domain with the high-speed analog to digital converter (ADC). Three features show the irreplaceable function of the digital coherent receiver:

1. Information can be encoded in both degree of amplitude and phase, which realizes the adoption of multi-level modulation format [15];

2. The polarization-multiplexed signals are able to be de-multiplexed in digital domain by finite-impulse-response (FIR) filter, which doubles the fiber capacity [16];

3. Digital signal processing (DSP) technique is applicable to mitigate the optical impairments, which eliminates the requirement of bulky chromatic-dispersion compensation modules [17, 18].

The digital coherent receiver is a great leap for the technique evolution in optical fiber research. It intrigues the extensive researches of DSP algorithm related to optical fiber communication for better system performance.

1.1.2 Next generation optical network over 100G

Over the past decades, the world has witnessed the explosive growth of Internet traffic. Fig. 1.3 shows the fiber system capacity increase in the past and prediction for the next decade [19, **?**]. Each evolution forward of the Internet exhausts the Internet traffic, and demands higher speed for the backbone of the Internet − the optical fiber communication network .

Over the past 10 years, the capacity of optical fiber link has been almost doubled every year, an increase by three orders of magnitude. The capacity of a single carrier channel has evolved from 10-Gbit/s to 100-Gbit/s [20, 21, 22]. The Internet traffic is

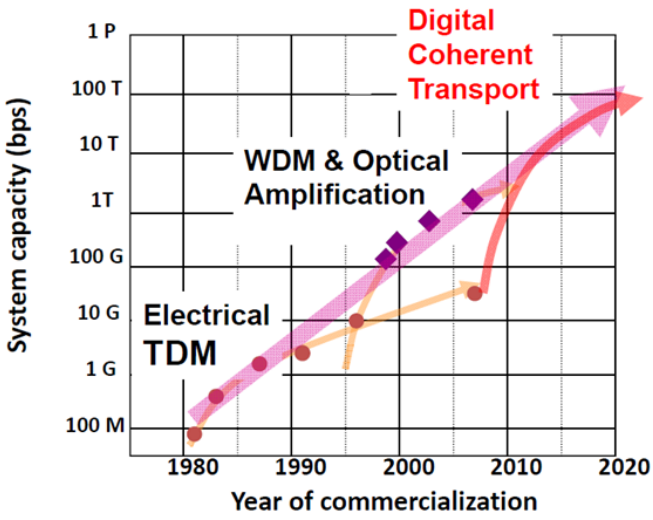

Figure 1.3: Capacity increase of fiber system in the past decades and prediction for the next decade

about to grow at the pace of 34% annually to meet the surging demands from mobile device, Internet video to TV and on-line video sharing.

To meet the future demand of Internet traffic, three possible directions have been proposed for the next generation of optical network over 100G:

- High-order modulation format in coherent communication system [23]
- Multi-mode and multi-core fiber transmission [24]
- Superchannel system with Nyquist spectrum or OFDM [25]

The proposal using high-order modulation formats (such as 16-QAM or 64-QAM) requires no modifications to the current system configuration of 100G optical network and increases the capacity by the improvement of spectrum efficient (SE). In such a case, the bits transmitted per symbol are increased as shown in Fig. 1.4(a). Under the current 25-GBaud optical system, DP-16QAM scheme can realize a 200-Gbit/s single channel capacity. Along with the improvement in electronics, it's promising to realize 400G optical network system in the near future. However, fiber-nonlinearity

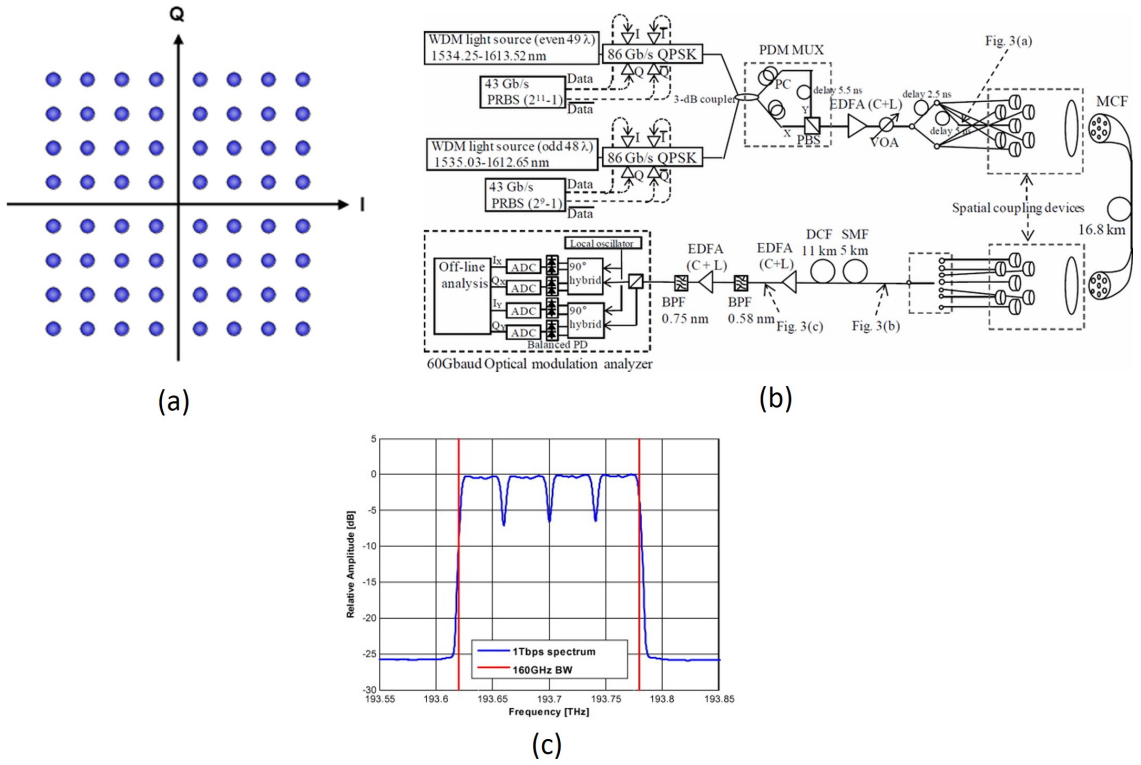

Figure 1.4: Proposals for next generation optical network over 100G: (a) 64-QAM modulation format; (b) schematic diagram of multi-core fiber system; (c) spectrum of high capacity system using superchannel method

is much severer in such systems, because high-order modulation format requires high signal power to maintain required signal-to-noise ratio (SNR).

In multi-mode and multi-core fiber system, the signals are transmitted on different modes to improve the fiber capacity, and there are multiple cores capsuled in one fiber to improve the fiber capacity. For the superchannel system, ultra-wide spectrum window is used for one channel transmission instead of 50GHz-fixed grid. These two systems are illustrated in Fig. 1.4(b) and (c), respectively. In both cases, The signal power issue occurs to such system as well and it's ultimately limited by fiber nonlinearity [26].

To achieve the next generation of optical network over 100G, fiber nonlinearity

becomes the ultimate factor limiting the system reach and capacity.

1.2 Works of the Thesis

To alleviate the fiber-nonlinearity distortion in optical fiber communication system, we propose a novel polarization-diversity scheme utilizing the mutual phase-conjugation signal. The method tends to solve the NL distortion problem in an optical manner without the additional computational requirement on DSP circuit.

There are two methods related to the mutual phase conjugation scheme in this work.

1.2.1 Mutual phase-conjugation method

We use the mutual phase conjugation scheme for the fiber-nonlinearity mitigation in coherent fiber systems. This method realizes NL mitigation by dissipating original signal power into two polarization modes. It provides 3-dB NL power tolerance improvement and no huge modification of the conventional coherent fiber system. We hereafter call this method the mutual phase conjugation (MPC) method.

Most previous research works focus on the DSP algorithm for the fiber-nonlinearity mitigation. However due to the intensity of the computational requirement, these fiber-nonlinearity mitigation algorithms are either impractical for real-time implementation or poor performance. We succeed in alleviating the fiber nonlinearity using the optical fiber, realizing 3-dB intrinsic NL power tolerance improvement. Because the NL mitigation is realized in an optical manner, it's ready for real-time implementation.

Three factors contribute to the NL power tolerance improvement: dissipation of the original signal power into two polarization modes; No deterioration of the linear signal to noise ratio; No extra cross-phase modulation effect between the signals on two orthogonal polarization modes. Combined these three factors, the nonlinear distortion is alleviated by over 3 dB in comparison to the single-polarization (SP) scheme and the dual-polarization (DP) scheme. It provides additional SPM mitigation effect

around 1 dB, which is stemmed from the anti-correlation of conjugation between the MPC signals in the initial spans.

1.2.2 Parallel back-propagation method

We use the pre-dispersion mutual phase-conjugation scheme to further mitigate the fiber nonlinearity. In addition to the intrinsic 3-dB improvement based on the mutual phase-conjugation method, the SPM mitigation effect is significantly improved with highly-effective nonlinearity-mitigation pattern. We hereafter call this method *the parallel back-propagation method*

The parallel back-propagation method generates the fiber-nonlinearity mitigation pattern in a similar way of the back-propagation method. Therefore the nonlinearity-mitigation effect outperforms all the DSP algorithms for fiber-nonlinearity mitigation. Through extensive simulations, we found the fiber nonlinearity is reduced by over 15 dB independent of the modulation format when the signal power is below 8 dBm. The optimal signal power is improved by 7 dB, which allows the use of high-order QAM and better system performance for ultra-long optical communication.

Besides the highly-effective fiber-nonlinearity mitigation result, the parallel back-propagation method is ready for real-time system implementation. The generation of the fiber-nonlinearity mitigation pattern is executed parallel with the original signal transmitted, and there is no extra computational requirement for the implementation of the pre-dispersion mutual phase-conjugation scheme. Both the transmitter and receiver requires no additional hardwares.

1.3 Organization

This thesis is organized into 6 chapters to explain the details of principle related to our NL mitigation methods and the demonstrations of both simulations and experiments. The background information, the research trend overview and the general objective are talked about in Chapter 1.

In Chapter 2, we first introduce main optical impairments in fiber communication

system, along with the conventional back-propagation method for optical impairment mitigation. Then, the principle of operation for the digital coherent receiver is explained, and the conventional DSP algorithms for optical impairment mitigation are reviewed in this part.

In chapter 3, we explain the principle of operation of the mutual phase conjugation method and the PBP method. We conduct both conceptual and analytical deduction to provide a general guideline for the optical system design in fiber-nonlinearity limited system.

In chapter 4, the simulation results are presented. The 3-dB intrinsic nonlinearity improvement is proved by extensive simulations based on mutual phase-conjugation scheme, and the PBP method is studied with impractical optical parameters for the verification of the principle of operation. Highly effective NL mitigation effect is verified for the PBP method.

In chapter 5, we discuss the experiment results of the mutual phase conjugation method and the PBP method.

In chapter 6, we conclude this thesis and list possible future works in terms of the mutual phase-conjugation scheme.

Chapter 2

Background knowledge

In this chapter, we reviewed the background knowledge for understanding the fiber-nonlinearity mitigation in coherent optical communication. The knowledge of waveform propagation function and the digital coherent receiver is essential for the understanding of fiber-nonlinearity mitigation. We deduce the principle of operation for the conventional and digital back-propagation method after the understanding of above two parts of critical knowledge.

In the following two sections, we first describe the nonlinear Schrödinger equation (NLSE) and deduce the optical impairments. Based on the knowledge on NLSE, we explain the principle of conventional back-propagation method for fiber-nonlinearity mitigation. Then the principle of the digital coherent receiver is introduced, followed by the DSP algorithm for optical impairments mitigation and digital back-propagation for fiber-nonlinearity mitigation. We analyze the disadvantages of the two methods, and propose the features for an effective and practical NL mitigation method.

2.1 Back-propagation method for fiber-impairment mitigation

In this section, we review the mathematical model NLSE for the lightwave propagation in single-mode fiber, and deduce the optical impairments against optical

communication. The conventional back-propagation method designed for the optical-impairment mitigation is discussed in the perspective of principle of operations and system implementation.

2.1.1 Optical impairments

The lightwave propagation through a single-mode fiber is described by the nonlinear Schrödinger equation (NLSE) [27]. For simplicity, here we consider the single polarized scheme. The NLSE is described as

$$\frac{\partial E_x}{\partial z} = (-\frac{1}{2}\alpha + j\beta_2\frac{1}{2}\frac{\partial^2}{\partial t})E_x - j\gamma\|E_x\|^2E_x \tag{2.1}$$

where the $E_x(z,t)$ is the electrical field of the transmitted signal at the location z and time slot t. The α, β_2 and γ represent the loss coefficient, the group-velocity dispersion (GVD) parameter and the fiber nonlinear coefficient, respectively. The GVD parameter is a wavelength dependent parameter centered at ω_0 as,

$$\beta_2 \equiv \beta_2(\omega_0) = \frac{d^2\beta}{d\omega^2}|_{\omega=\omega_0} \tag{2.2}$$

In optical system design, the chromatic dispersion (CD) coefficient is more commonly used. The relation between the GVD parameter β_2 and the CD coefficient D is

$$D = -\frac{2\pi c}{\lambda^2}\beta_2 \tag{2.3}$$

The fiber nonlinear coefficient γ is defined as,

$$\gamma = \frac{n_2\omega_s}{cA_{eff}} \tag{2.4}$$

where n_2 is the fiber nonlinear refractive index. ω_s is the angular optical frequency at the signal wavelength v_s, which is defined as $\omega_s = 2\pi v_s$. The A_{eff} is the fiber

effective area, defined as

$$A_{eff} = \frac{(\int\int_{-\infty}^{\infty} \|F(x,y)\|^2 dxdy)^2}{\int\int_{-\infty}^{\infty} \|F(x,y)\|^4 dxdy} \tag{2.5}$$

where $F(x,y)$ is the mode field transverse distribution.

In the polarization-multiplexed system, both lightwaves on the two orthogonal-polarization modes contribute to the nonlinear term, while the GVD responds to the lightwave on each polarization state. The two-mode NLSE is described as,

$$\frac{\partial E_x}{\partial z} = (-\frac{1}{2}\alpha + j\beta_2 \frac{1}{2}\frac{\partial^2}{\partial t})E_x - \frac{8}{9}j\gamma(\|E_x\|^2 + \|E_y\|^2)E_x \tag{2.6}$$

where the E_x and E_y are the electrical field of the transmitted signal on x-/y- polarization mode, respectively.

According to the Eq. 2.1, the waveform evolution of an optical lightwave propagated through SMF is composed by linear part L and nonlinear part N, respectively. The Eq. 2.1 is re-written as

$$\frac{\partial E_x}{\partial z} = L \cdot E_x - N \cdot E_x \tag{2.7}$$

$$L = -\frac{1}{2}\alpha + j\beta_2 \frac{1}{2}\frac{\partial^2}{\partial t}, N = -j\gamma\|E_x\|^2 \tag{2.8}$$

The linear part L is responsible for the signal energy loss and the GVD effect.

The signal energy loss is determined by the loss coefficient α and the fiber length signal transmitted

$$P_{out} = P_{in} exp(-\alpha L) \tag{2.9}$$

It is customary to express α in units of dB/km by using the relation

$$\alpha(dB/km) = -\frac{10}{L} log_{10}(\frac{P_{out}}{P_{in}}) \tag{2.10}$$

The fiber loss is generally compensated for periodically by EDFAs cascaded after each fiber loop, which introduces Amplified Spontaneous Emission (ASE) noise degrading

the signal quality.

The group velocity dispersion (GVD) is the wavelength dependence of the group velocity, which leads to an alternation of the pulse shape and inter-symbol interference (ISI). In frequency domain, the transformation of signal E_x is

$$E_x(\omega, z) = E_x(\omega, 0) \cdot exp(-j\frac{1}{2}\beta_2\omega^2 z) \tag{2.11}$$

Eq. 2.11 shows the GVD adds phase rotation in frequency domain according to the frequency ω and distance z. In time domain, it is equivalent to phase velocity according to different wavelength. The difference in phase velocity causes waveform transformation. If the GVD is not effectively controlled or mitigated, the system reach will be ultimately limited by GVD.

The nonlinear part N is responsible for the nonlinear phase shift, causing self-phase modulation (SPM), cross-phass modulation (XPM), and four-wave mixing (FWM). The solution for the nonlinear part is simple,

$$E_x(z, t) = E_x(0, t)exp(-j\gamma\|E_x(0, t)\|^2 z) \tag{2.12}$$

where $E_x(0, t)$ and $E_x(z, t)$ are the electrical field of the lightwave at 0 and z position, respectively. The nonlinear part simply adds phase shift to the signal at each time slot as a function of the signal power $\|E_x(0, t)\|^2$. When considering the nonlinear phase shift in frequency domain, it behaves as signal modulation where new frequency components are generated via the intensity dependency of the phase of the signal transmitted.

In the practical optical fiber system, the interaction of the GVD and NL effect is complicated and places tremendous difficulties to recover the original signal, because the alternation of signal waveform leads to variations of phase shift. The waveform transformation is not applicable for analytical deduction due to the interaction between this two effects [28]. We hereafter call the degradation caused by the interaction between the GVD and the nonlinear phase as *fiber-nonlinearity distortion*.

Although the signal energy loss can be simply compensated for by EDFAs, the GVD and the fiber-nonlinearity distortion ultimately limit the system performance

which requires novel proposals to release the system limitation.

2.1.2 Conventional back-propagation method

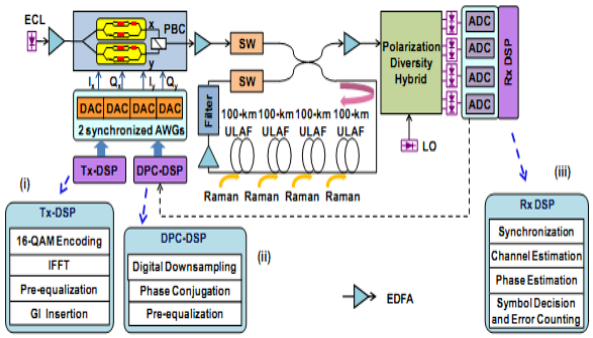

Figure 2.1: Schematic diagram for midway phase conjugation method of a 16-QAM system based on digital phase conjugation

To exclude the influence of GVD and the fiber-nonlinearity distortion, back-propagation method was proposed to remove the optical impairments in a reversed signal-evolution manner.

The complex conjugation of Eq. 2.1 yields

$$\frac{\partial E^*}{\partial(-z)} = (\frac{1}{2}\alpha + j\beta_2\frac{1}{2}\frac{\partial^2}{\partial t})E^* - j\gamma\|E_x\|^2E^* \tag{2.13}$$

We assume that the system length is L. In such a case, if the power distribution along the link is ignored as $\alpha : 0$, the signal is re-transmitted in the backward direction from the output at $z = L$, and the evolution of $E_x(L,t)^*$ experiences the exact reversed optical process, in comparison to the forward direction transmission. we obtain $E_x(0,t)$ at the input end by taking complex conjugation to restore the signal. This undo process is called *back propagation* and can restore the initial waveform at the input end.

In practical scheme, the undo process of the GVD and the fiber-nonlinearity distortion is executed through midway phase-conjugation method [29], shown in Fig. 2.1.

The transmitted signal is phase-conjugated at the middle point of the whole transmission link as E_x^*. The phase-conjugated signal E_x^* is then transmitted through the second half of the link with the same characteristics of the first part. The dispersive/nonlinear impairments generated along the first half of the link are undone along the second half of the link in a back-propagation manner. As the power-loss map is not possible to reversed in a practical system, the undo process is not perfect as the analysis of back-propagation scheme.

The operation of phase-conjugation at the middle point can be realized either in a optical manner which uses wavelength convertors based on four-wave mixing technique, or in a electrical manner which deploys coherent detection. Both methods for phase-conjugation degrade the signal quality, and the requirement of exerting the phase conjugator at the middle point of the whole fiber link significantly limits the flexibility for system design.

2.2 Principle of the digital coherent receiver

The digital coherent receiver constructs the cornerstone of today's high-speed fiber communication network. Two irreplaceable features are intrinsic for the digital coherent receiver:

- Full utilization of all degrees of freedoms in optical domain, including the phase, the amplitude, and the polarization;
- Conversion of the full information in optical domain into digital domain, which enables impairment mitigation using high-speed DSP circuit.

In this section, we introduce the configuration of the coherent receiver, the principle of the coherent detection and the algorithms of the DSP circuits.

2.2.1 Configuration of coherent transceiver

The configuration of the coherent transceiver differs from conventional IM-DD fiber system in terms of the devices for transceiver construction and design. The conventional transceiver for IM-DD system requires only intensity modulator for signal

modulation and photo-diode (PD) for detection of signal intensity. The design of coherent transceiver requires multiple Mach-Zehnder Modulators (MZMs) and PDs for signal de-/modulation [30]. The schematic diagram of coherent transceiver is shown in Fig. 2.2.

For the transmitter, the coherent transceiver utilizes a pair of MZMs to encode the desired signal on amplitude and phase. The incident light is divided into two branches. The sub-MZM in each arm imprint two independent bit streams on the incident light. In the case of QPSK, the two signals are modulated into binary PSK. Then another MZM is used to introduce a constant 90 ° phase shift between two signals. The two mutual-quadrature signals are combined in the output coupler to produce a M-QAM modulation format. The polarization beam coupler (PBC) combines the two streams of signals at same wavelength onto two polarization modes to form a polarization-multiplexed signal.

For the receiver, first a local oscillator (LO) is used to interfere with the received signal. The polarization beam splitter divides the incident light into two orthogonal polarization mode. A 90 ° optical hybrid shifts the incident light with 90 ° to detect both IQ components of the signal light. Then the balanced detector helps to cancel the DC component of the detected signal and enhance the quadrature pair. Sampled by high-speed analog to digital convertor, the full information in optical domain is converted into digital domain and be able to be processed by DSP for impairment mitigation.

2.2.2 Principle of coherent detection

The principle of the coherent receiver is based on the interference of lightwave between the incident signal and the LO. There are two types of coherent detection: heterodyne and homo-dyne. In this section we focused on the explanation of the homy-dyne coherent receiver.

The incident signal and the LO are described as,

$$E_s(t) = A_s(t)exp(j\omega_s t) \tag{2.14}$$

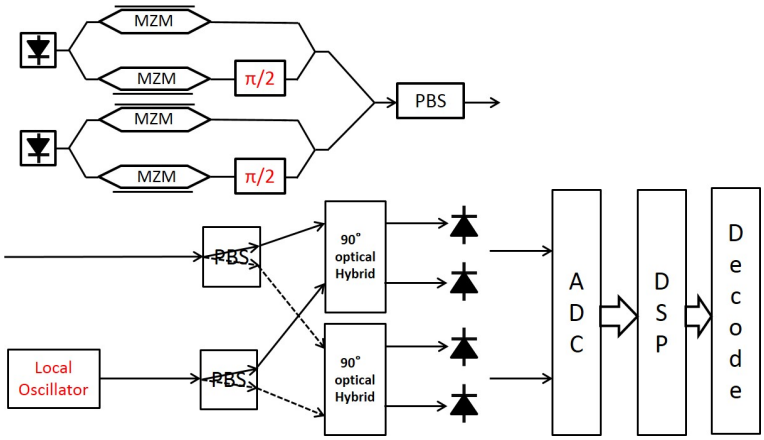

Figure 2.2: Schematic diagram of coherent transceiver

$$E_{LO}(t) = A_{LO}(t)exp(j\omega_{LO}t) \tag{2.15}$$

where $A_s(t)$ and $A_{LO}(t)$ is the modulated and the LO signal, respectively. ωs and ω_{LO} are the angular frequency for the incident light and the LO, respectively.

The two interfered lightwaves are detected by balanced detector after a 180 ° phase shift imposed by the optical coupler. The electric fields incident on the upper and lower PDs are expressed as,

$$E_1 = \frac{1}{\sqrt{2}}(E_s + E_{LO}) \tag{2.16}$$

$$E_2 = \frac{1}{\sqrt{2}}(E_s - E_{LO}) \tag{2.17}$$

Therefore, the output photocurrents of the two PDs are,

$$I_1(t) = \frac{R}{2}[P_s + P_{LO} + 2\sqrt{P_s P_{LO}}cos\{\omega_{IF} + \theta_{sig}(t) - \theta_{PN}(t)\}] \tag{2.18}$$

$$I_2(t) = \frac{R}{2}[P_s + P_{LO} - 2\sqrt{P_s P_{LO}}cos\{\omega_{IF} + \theta_{sig}(t) - \theta_{PN}(t)\}] \tag{2.19}$$

where R is the responsitivity of the PD. ω_{IF} is the wavelength difference between the incident light and the LO, where in homodyne coheret detection, $\theta_{sig}(t)$ is the information encoded on phase, and $\theta_{PN}(t)$ is the laser phase noise from both the

transmitter and the LO.

Then output of the 1st balanced detector in the homo-dyne coherent receiver is recovered with no DC component and converted back to baseband. Similarly, the output of the other balanced detector is deducted in a similar manner, which procudes the quadrature component of the original signal. The two outputs are expressed as

$$I_I(t) = I_1(t) - I_2(t) = 2R\sqrt{P_s P_{LO}}cos\{\theta_{sig}(t) - \theta_{PN}(t)\}] \tag{2.20}$$

$$I_Q(t) = I_1(t) - I_2(t) = 2R\sqrt{P_s P_{LO}}sin\{\theta_{sig}(t) - \theta_{PN}(t)\}] \tag{2.21}$$

The two output $I_I(t)$ and $I_Q(t)$ reconstruct the original complex amplitude signal as

$$I_c(t) = I_I(t) + jI_Q(t) = R\sqrt{P_s P_{LO}}exp\{j(\theta_{sig}(t) + \theta_{PN}(t)\} \tag{2.22}$$

The above analysis also applies to the polarization-multiplexed system. Assuming the alignment of the polarization state of the incident signal and the LO light, the incident signals on the orthogonal polarization modes are interfered by the LO light-wave. The interfered signals are detected coherently by the four pairs of balanced detectors. According to the system configuration illustrated in Sec.2.2.1, the detected signals are

$$I_c(t) = I_{PD1}(t) + jI_{PD2}(t) \tag{2.23}$$

$$I_c(t) = I_{PD3}(t) + jI_{PD4}(t) \tag{2.24}$$

After the high-speed analog-to-digital convertor, the full information in optical domain is converted into digital domain, which enables the implementation of digital signal processing for impairment mitigation.

2.2.3 Digital signal processing of coherent receiver

The DSP circuit in the digital coherent receiver enables a high performance and reliability fiber system with reduced cost. It electronically equalizes the received signal and eliminates the optical impairments. This feature eliminates the use of bulky dispersion-compensation fiber (fiber) and enables the signal multiplexing on

polarization mode.

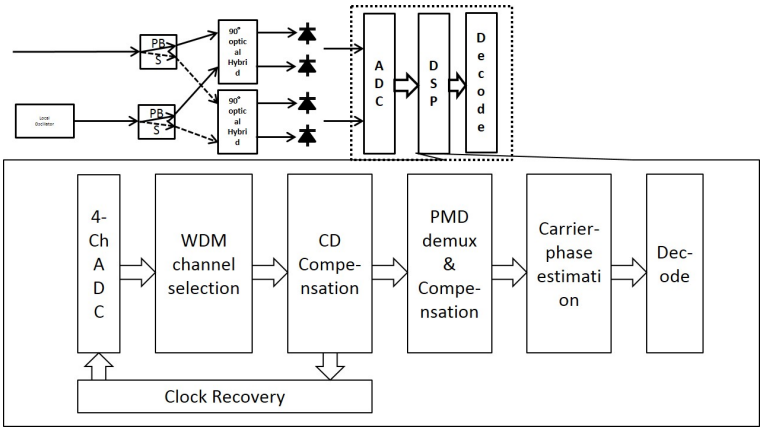

Figure 2.3: Process of DSP circuit

The DSP for the digital coherent receiver operates under the sequence to recover the received signal, as shown in Fig. 2.3:

- Sampling and digitizing the down-converted signal by high-speed ADC
- CD compensation
- Polarization alignment and de-multiplexing
- Equalization for residual CD, PMD, PDL, and clock recovery
- Carrier phase estimation
- Symbol discrimination

In the process of high-speed ADC, the sampling frequency is required to be twice as the signal highest frequency to avoid the aliasing effect according to the Nyquist sampling theorem [31].

For randomly time-varying optical impairments such as PMD and PDL, it requires adaptive mechanism to remove such fluctuations. The finite-impulse-response (FIR) filter is a promising solution to adapt such time-varying factors.

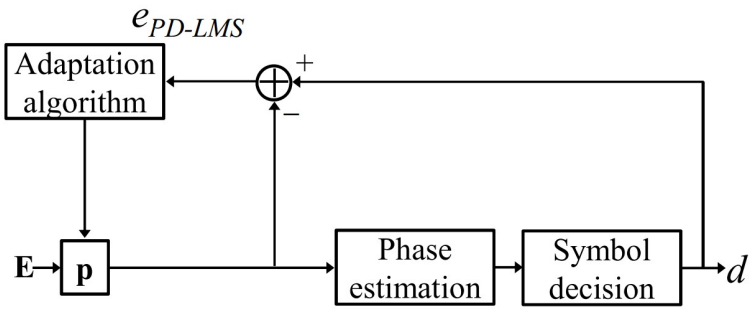

Figure 2.4: Flow chart of the FIR filter

If we neglect the NL effect, the fiber is a linear channel modeled as a concatenation of CD, PMD, and PDL as

$$H(\omega) = D(\omega)U(\omega)KT \tag{2.25}$$

where $D(\omega)$, $U(\omega)$, K, and T represent the CD, PMD, PDL, and the birefringence of the fiber, respectively.

For the mitigation of such optical impairments and recover the original signal, it's desired to seek the inverse matrix of $H(\omega)$ as

$$H_{eq}(\omega) \simeq H(\omega)^{-1} = \begin{pmatrix} h_{xx}(\omega) & h_{xy}(\omega) \\ h_{yx}(\omega) & h_{yy}(\omega) \end{pmatrix} \tag{2.26}$$

The transfer function $H_{eq}(\omega)$ is acquired through adaptive FIR filter based on either CMA or DD-LMS algorithm. Assume the vectors for x-/y- polarization are

$$E_x(n) = [x(n), x(n-1), x(n-2), ..., y(n-k-1)]^T \tag{2.27}$$

$$E_y(n) = [y(n), y(n-1), y(n-2), ..., y(n-k-1)]^T \tag{2.28}$$

where $x(n)$ and $y(n)$ is the sampled signal from x and y port of the coherent receiver. k is the number of taps of the FIR filter.

In such a system, the generation process of the tap coefficients are shown in

Fig. 2.4. The tap coefficients of the FIR filter based are updated as

$$h_{pq}(n+1) = h_{pq}(n) + \mu E_x(n)x^*(n) \tag{2.29}$$

$$h_{pq}(n+1) = h_{pq}(n) + \mu E_y(n)y^*(n) \tag{2.30}$$

where p and q is either x or y, and μ is the step-size parameter. In DD-LMS algorithm, the error estimation $e_x(n)$ and $e_y(n)$ is given as

$$e_x(n) = d_x(n) - E_x(n) \tag{2.31}$$

$$e_y(n) = d_y(n) - E_y(n) \tag{2.32}$$

where $d_x(n)$ and $d_y(n)$ are the decoded symbols. In CMA algorithm, the error estimation are given as

$$e_x(n) = (1 - \|E_x(n)\|^2)E_x(n) \tag{2.33}$$

$$e_y(n) = (1 - \|E_y(n)\|^2)E_y(n) \tag{2.34}$$

The tap coefficients are updated so as to recover the complex amplitudes to constant.

Note for the DD-LMS algorithm, a set of training symbols is required and after the training symbols, it switches to tracking mode for adaptive signal equalization. Instead of the drawback of the need for training symbol, DD-LMS algorithm is applicable to high-order modulation format while CMA algorithm is not.

After the convergence of the adaptive-FIR filter, the time-varying factors as PMD and PDL are adaptively mitigated and polarization de-multiplexing and residual CD compensation are performed simultaneously by the adaptive-FIR filter.

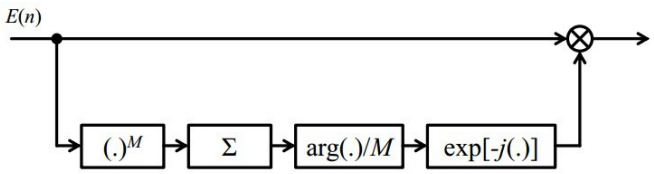

Figure 2.5: Block diagram of M-th power phase estimation algorithm

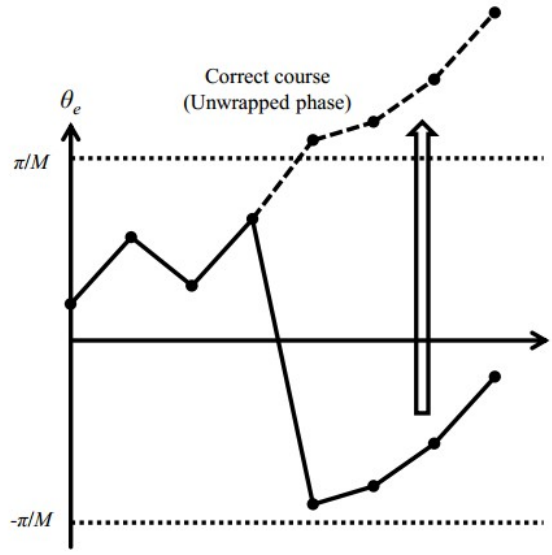

Figure 2.6: Phase jump correction during phase estimation

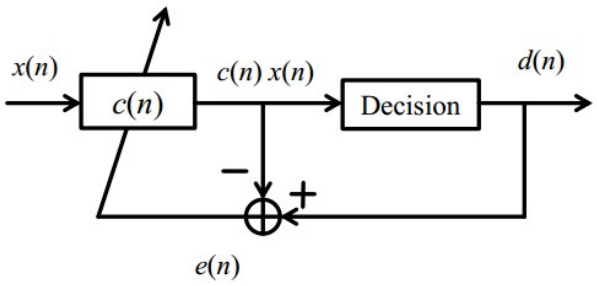

Figure 2.7: Block diagram of decision-feedback carrier-phase estimator

The carrier phase estimation is performed to minimize the influence of laser phase noise from the transmitter and LO [32, 33]. Because the linewidth of distributed feedback (DFB) laser varies much more slowly than the baudrate, the phase error from the laser source is possible to be minimized by averaging the phase noise of a bunch of symbols. Such method is call M-th power phase estimation method.

The procedure of M-th power phase estimation method is described in Fig. 2.5

for M-ary PSK signals: First the phase information θ_{sig} of the modulated signal is removed by taking M-th power of the received signal; Then, the phase noise θ_n is averaged to remove the fluctuations. The estimated phase error $\theta_e(n)$ is acquired by dividing the averaged phase noise by M

$$\theta_e n = arg[\sum_{m=-k}^{k} E(n+m)^M]/M \tag{2.35}$$

where $2k+1$ is the block length.

The estimated phase error θ_e has ambiguity of $2\pi/M$ as the absolute phase has not been determined. The phase ambiguity is avoided by differential coding.

The phase unwrapping is necessary when the estimated phase $\|\theta_e\| > \pi/M$. The unwrapping process is shown in Fig. 2.6.

In high-order QAM modulation phase, the signal phase is not equally spaced, which is not ideal for the implementation of M-th power method. To tackle such a problem, the LMS algorithm is adopted using one-tap coefficient.

Fig. 2.7 shows the schematic diagram of the phase estimator [34]. The phase error is minimized by one-tap coefficient $c(n)$ which gives phase rotation of the input signal $E_{in}(n)$,

$$E_{cr}(n) = E_{in}(n)c(n) \tag{2.36}$$

where $E_{cr}(n)$ is the output signal after carrier recovery.

The update of $c(n)$ is given as

$$c(n+1) = c(n) + \frac{\mu}{\|E_{in}(n)\|^2} e(n)x^*(n) \tag{2.37}$$

$$e(n) = d(n) - E_{cr}(n) \tag{2.38}$$

where $d(n)$ is the decoded symbol and e(n) is the error signal.

2.2.4 Digital back-propagation method

The back-propagation method can effectively perform the mitigation of fiber-nonlinearity distortion as explained in Sec. 2.1.2. However the requirement of a phase conjugator at the middle point of the fiber link ultimately limits its application. The digital back-propagation method is proposed tends to solve such problem.

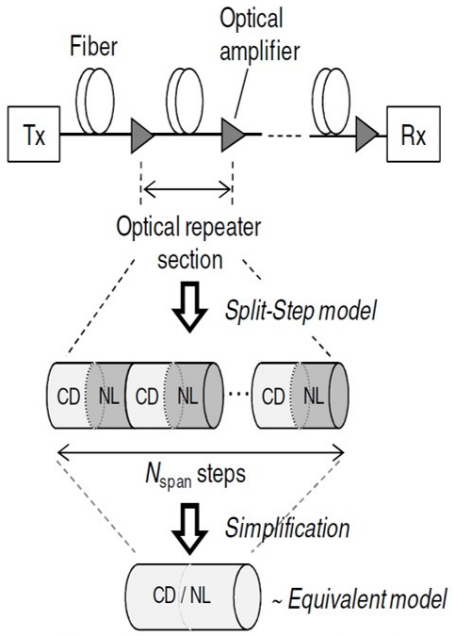

Figure 2.8: Block diagram of split-step method for digital back-propagation method

As the waveform transformation follows the NLSE as shown in Eq. 2.6, the split-step method can simulate the waveform evaluation numerically. Fig. 2.8 illustrates the general process of such method. First, the whole transmission is divided into short-fiber segments referred as split steps. In such short-fiber segments, the linear and nonlinear operations is calculated separately in an iterative manner. A large number of the fast Fourier transform (FFT) and its inverse operation, IFFT, is necessary to perform the iteration of split-step method. Such method is call the *digital back-propagation* (DBP) method.

Through iteration of such process, the final output of the fiber can be calculated precisely if the size of split steps is small enough. However, the number of

FFT/IFFT blocks is inversely with the size of split-step, and it places difficulties for practical utilization because the implementation of FFT/IFFT blocks requires extra time for computations. In order to obtain satisfactory NL mitigation effect, the number of FFT/IFFT operations has to be way beyond the state-of-art semiconductor technology for real-time operation. Moreover, the split-step method is based on the serial signal processing which is not suitable for hardware implementation.

Based on above reasons, the digital back-propagation method is not a practical candidate for fiber-nonlinearity mitigation.

2.3 Conclusion

In this chapter, we review the basic knowledge for understanding of the fiber-nonlinearity mitigation: the NLSE and the digital coherent receiver. Two conventional fiber-nonlinearity mitigation method are introduced in the perspective of principle and its pros and cons.

Based on the analysis of the two conventional fiber-nonlinearity mitigation, we summarize the featured requirements for an effective and practical NL mitigation method:

- highly effective mitigation effect to emancipate the fiber capacity from fiber nonlinearity;
- applicable for real-time implementation;
- no restriction of the system design;
- Independent of the modulation format;

We propose the mutual phase-conjugation scheme and the parallel back-propagation method to meet the above four requirements. In the following chapter, we explain the principle of operations of our methods for fiber-nonlinearity mitigation.

Chapter 3

Principle of the MPC methods

In this chapter, we explain the principle of operation of the proposed methods for fiber-nonlinearity mitigation. For the mutual phase-conjugation method, we first describe the system configuration and the receiver-end DSP algorithm, then the 3-dB intrinsic NL power tolerance improvement is elaborated in details. As an extension of the mutual phase-conjugation method, the parallel back-propagation method utilizes a similar system configuration to the one of mutual phase-conjugation. We focus on the explanation of the principle of operations of the parallel back-propagation method.

Based on the analyses of the principle of operations, the factors which have influence on the NL mitigation performance are deduced. Therefore, we provide the general guideline for the design of mutual phase-conjugation system and the parallel back-propagation method.

3.1 Mutual phase Conjugation Scheme

For practical nonlinearity mitigation, the diversity scheme is an attractive solution: the signal power is dissipated into multiple replicas, which are detected by multiple coherent receivers. In this scheme, the signal-to-noise ratio (SNR) can be restored by coherently processing multiple received signal replicas, while the dissipation of the original signal power into several replicas leads to the reduction of the signal power

of each replica; therefore, SPM-induced waveform distortion during fiber propagation is alleviated.

We utilize a polarization-diversity based scheme to realize the fiber-nonlinearity alleviation. In such a case, a single polarization-diversity coherent receiver can process the signals. We call this method the *mutual phase-conjugation* (MPC) method.

3.1.1 Configuration for the Mutual Phase Conjugation method

The system configuration for the MPC method is based on conventional coherent fiber system, as shown in Fig. 3.1.

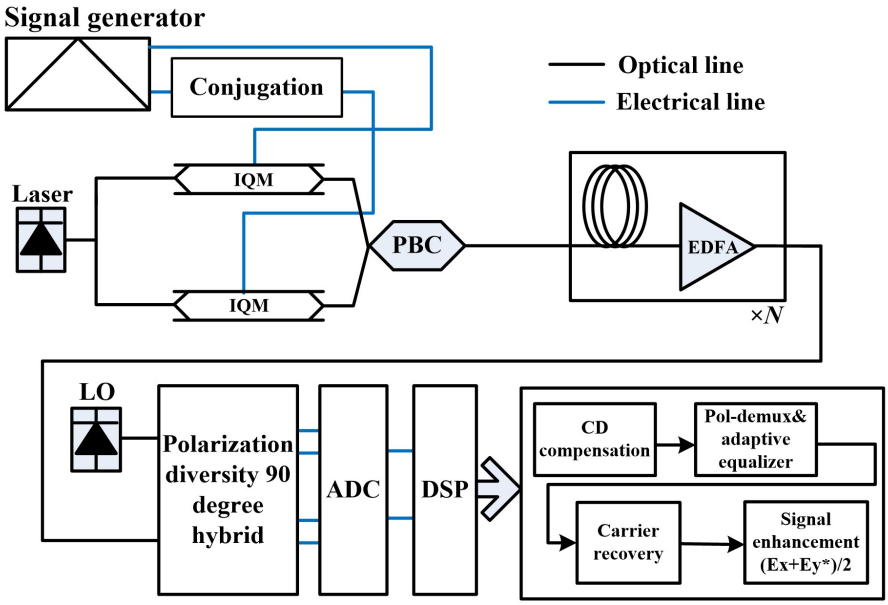

Figure 3.1: Configuration of a polarization-diversity mutual phase-conjugation scheme

At the transmitter, a pair of optical IQ modulators (IQMs) is used to generate a desired signal and its phase-conjugated replica. Only one signal generator is required for the inputs of the IQMs, the operation of phase-conjugation is realized by switching the I-/Q- input for the IQMs. The modulated signals are transmitted simultaneously by PDM. When complex amplitudes of horizontal and vertical polarization modes

are denoted as $E_x(z,t)$ and $E_y(z,t)$, respectively, the y-polarization component in our scheme is given as the phase-conjugation of the x-polarization component at the input (z=0), that is, $E_y(0,t) = E_x^*(0,t)$.

At the receiver ($z = L$), the general procedures of the MPC receiver are similar to that of the conventional coherent receiver. Here the coherent receiver is implemented in a homo-dyne manner, where the wavelength of the LO ω_{LO} is centered at the wavelength of the received signal ω_{sig}. After interfered with LO E_{LO}, the received signals $E_x(L,t)$ and $E_y(L,t)$ are down-converted to baseband and sampled by high-speed ADCs for DSP.

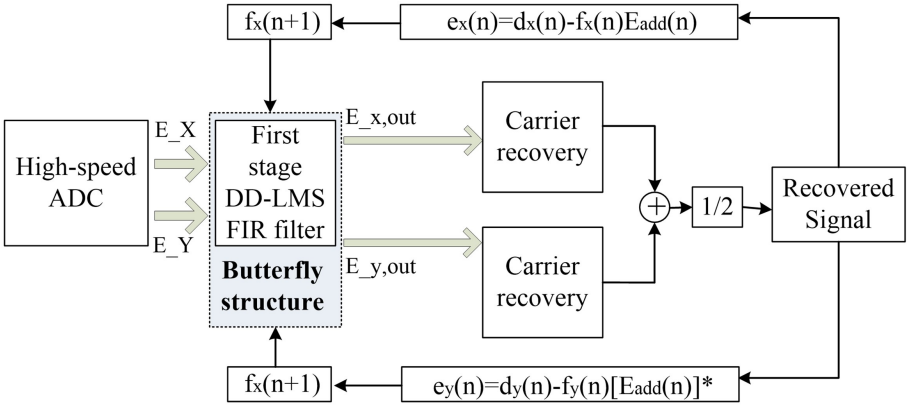

Figure 3.2: DSP circuit for the mutual phase-conjugation method

The DSP circuit is shown in Fig. 3.2. The input signals are compensated for CD with fixed value, and then polarization de-multiplexed with finite-impulse-response (FIR) filter using the constant modulus algorithm (CMA) or decision-direct least-mean-square (DD-LMS) algorithm, which simultaneously performs the residual CD compensation and clock recovery. After the carrier estimation which is performed by M-th power algorithm or DD-LMS algorithm, we have the output of two signal from each polarization E_{x-out} and E_{y-out}. The NL-mitigated signal $E_{mpc-out}$ is calculated by averaging the two signals

$$E_{mpc-out} = \frac{E_{x-out} + E_{y-out}}{2} \tag{3.1}$$

The conventional DD-LMS algorithm is modified for the MPC scheme for better pol-demultiplexing and signal recovery. The conventional DD-LMS algorithm is shown in Fig. 2.4 in Chapter 2. The error signal e_{DD-LMS} for the update of the tap vector p(n+1) is calculated from the signal E_{x-out} and E_{y-out}. Because E_{x-out} and E_{y-out} are NL-distorted, they lead to inaccurate for the tap vector of the DD-LMS algorithm. In the modified DD-LMS algorithm for MPC scheme, the error signal e_{DD-LMS} is updated from d_n the decision signal, and $E_{mpc-out}$ the output signal after NL mitigation, as shown in Fig. 3.2. The error signal therefore eliminates the influence from NL distortion and leads to the update of the tap vectors p(n+1) more accurate.

3.1.2 Principle of the Mutual Phase Conjugation method

The MPC scheme brings nonlinear power tolerance improvement by 3 dB. This is explained in the following two aspects.

First, the linear SNR of the MPC scheme is not deteriorated in comparison to that of the SP scheme. As two polarization modes are used for the original signal and its MPC replica transmission, the amount of ASE noise is as twice large as that in the SP scheme. Assume the noise density is N_0, the noise imposed on signal in the SP scheme is $B \cdot N_0$, where B is the required signal bandwidth. The SNR of the SP scheme is,

$$SNR_{sp} = \frac{P_{sp}}{B \cdot N_0} \tag{3.2}$$

where P_{sp} is the transmitted signal power.

For MPC scheme, as two polarization modes are used for signal transmission, the polarizer is not applicable for noise reduction by blocking one polarization mode. Thus the amount of noise on the received signal is $2B \cdot N_0$. Meanwhile, the total signal power for the MPC signals remains the same as the one of the SP scheme: $P_{sp} = 2P_{mpc}$, where P_{mpc} is the power of signal on one polarization tributary in the MPC scheme, as shown in Fig 3.3. At the coherent receiver of the MPC scheme, the correlation between the two MPC signals is recovered after the operation of conjugation and CD compensation. Therefore, the two signals can be added coherently which boost the

signal power by four times. The calculated SNR for the MPC scheme is

$$SNR_{mpc} = \frac{4P_{mpc}}{2B \cdot N_0} = \frac{P_{sp}}{B \cdot N_0} = SNR_{sp} \tag{3.3}$$

This indicates that the linear SNR for the MPC scheme manages to keep the same as that of the SP scheme despite the double of the amount of ASE noise.

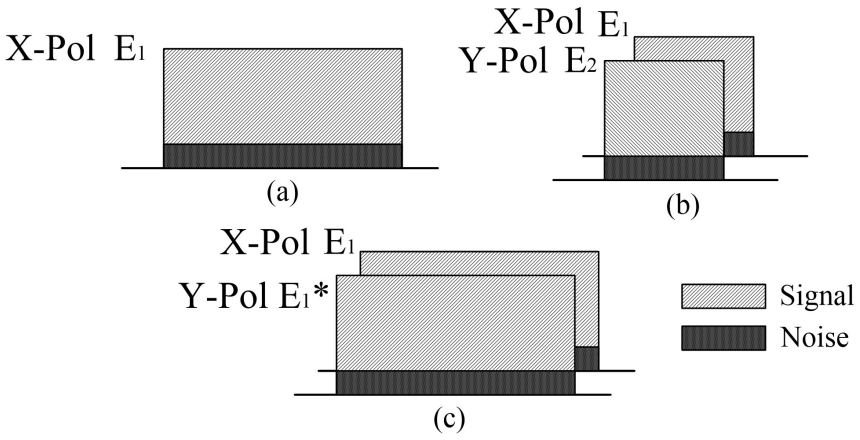

Figure 3.3: Illustration of the spectrum from the perspective of signal and noise power, (a) SP (b) DP (c) MPC

Second, cross phase modulation (XPM) between the two polarization modes is reduced by half compared with SPM in comparison to that of the SP scheme. In the MPC scheme, the signal power on each polarization tributary is 3 dB lower than that of the SP scheme. Furthermore, XPM between the MPC signals on two polarization modes are de-correlated by conjugation. In such a case, XPM between the two decorrelated polarization modes is half the amount of SPM in the SP transmission system as far as the total power and the bit rate are the same. We can expect 3-dB improvement of NL tolerance with our scheme independently of the symbol rate, the transmission distance, and the modulation format.

Additionally, there is an extra SPM mitigation effect stemming from mutual phase-conjugation. Note at$z = 0$ the two MPC signals are anti-correlated $E_x = E_y^*$, where E_x is the original signal and E_y is the MPC replica. In the first several spans, the anti-correlation between the two MPC signals is preserved and the NL phase rotation

can be canceled by phase-conjugation method. However, the dispersion pattern for the two MPC signals is different because the spectrum for the MPC replica is the reversed version in comparison to that of the original signal. Therefore, the SPM mitigation effect from phase-conjugation is minor, around 1 dB for QPSL system.

Taking these two NL mitigation effects into account, we can enjoy more than 3-dB improvement of NL tolerance.

As an alternative approach to transmit a signal at the same bit rate, we can choose the dual-polarization (DP) scheme, where two independent tributaries at the half symbol rate are transmitted. However, the NL reduction is less than 3 dB because of the lower symbol rate. Moreover, we cannot achieve the NL cancellation effect; therefore, the improvement of NL tolerance is smaller than 3 dB.

3.2 Parallel Back-Propagation

In the MPC scheme, the fiber-nonlinearity distortion is alleviated by disspipating the original signal power into two polarization modes. The 3-dB intrinsic NL power tolerance improvement is prominent in comparison to other DSP algorithms for NL mitigation, but the contribution from SPM mitigation is minor owing to the different dispersion pattern of two MPC signals. To further improve the NL mitigation effect, the PBP method is used to mitigate SPM distortion.

3.2.1 Limitation of SPM mitigation of MPC scheme

In MPC scheme, the SPM mitigation effect is mere for the disruption of anti-correlation during the fiber transmission. The calculation of the cross-correlation is shown in Fig. 3.4 The anti-correlation can be evaluated by the normalized cross-correlation between the intensity of two MPC signals, which is defined as c_{xy}

$$c_{xy} = \frac{1}{R} \sum_{n=0}^{n=N-1} \|x_n\|^2 \|y_x\|^2 \tag{3.4}$$

$$R = \sum_{n=0}^{n=N-1} \|x_n\|^2 \cdot \|x_n\|^2 \tag{3.5}$$

where N is the length of the tested data, and R is the auto-correlation of the tested data. In MPC scheme, the input signal for x_n and y_n is E_x and E_y, respectively. As these two signals are mutual phase-conjugated, theire auto-correlation R is the same.

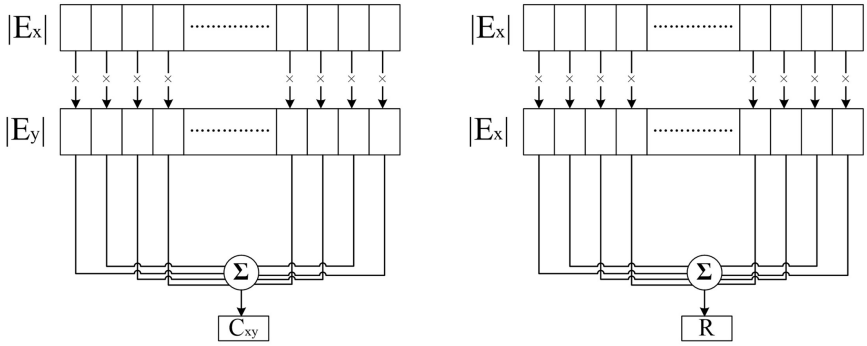

Figure 3.4: Calculation of normalized cross-correlation

We calculated the evolution of normalized cross-correlation between the MPC signals in a dispersive channel. The dispersive term is designed according to Eq.2.11. The dispersive coefficient β_2 is set to be 17ps/nm/km. Fig. 3.5 shows the sharp descend of the normalized cross-correlation between the MPC signals, which indicates that the anti-correlation is quickly disrupt. In the designed simulation scheme, the anti-correlation disappares after 100-km transmission.

In general, higher dispersive coefficient is desired for fiber-nonlinearity limited system because fast signal variation averages the nonlinear phase shift and therefore reduces the NL distortion. In MPC scheme, the improvement of the SPM mitigation becomes a dilemma in the perspective of the design of dispersion.

This situation requires us to seek different routes instead of utilize anti-correlation from conjugation for SPM mitigation. The PBP method is designed under such logic, where the NL mitigation pattern is generated in a back-propagation manner through the fiber.

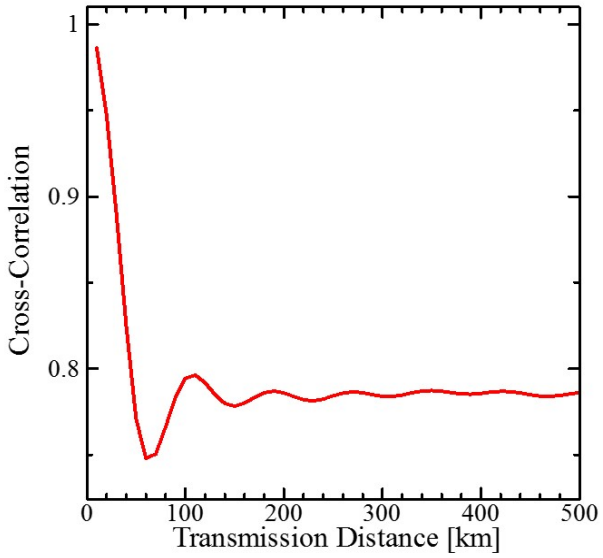

Figure 3.5: Normalized cross-correlation bewteen original signal and its MPC replica in a dispersion-only fiber channel

3.2.2 Configuration for the Parallel Back-Propagation method

The configuration for the PBP method is based on the pre-dispersion MPC scheme. It adds no extra optical devices upon the MPC scheme and requires minor modification in the digital circuit. Fig. 3.6 labels the modifications in red block.

The original data as two binary sequences are modulated into QPSK or higher modulation format. Such modulated signal is then processed with DSP algorithms such as pre-disperison and addition of perturbation term. The processed signal E_x is replicated into two sets for signals on X-/Y- polarization mode. In our case, E_x is directly imposed on the IQM for X-polarization. For the input of IQM for Y-polarization, the input signal E_y is pre-dispersed and taken phase-conjugation

$$E_y(t,0) = E_x(t,0) * H(t,L) \tag{3.6}$$

where $H(t,Z)$ represents the transform function of dispersive term described in Eq. 2.11, and $*$ denotes the operation of convolution.

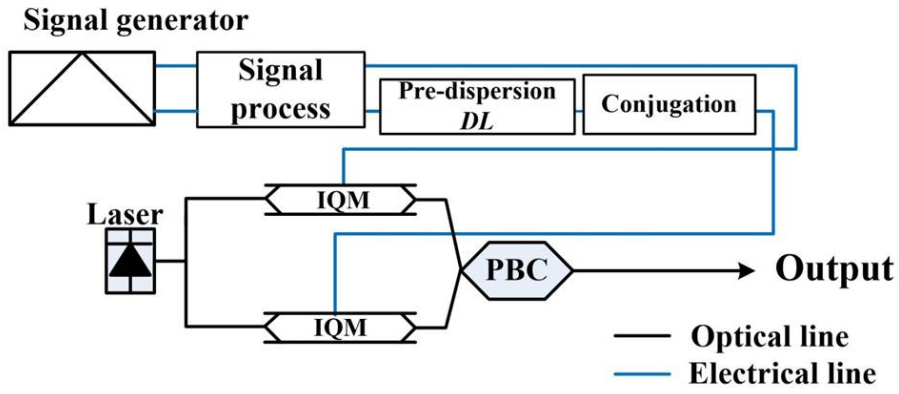

Figure 3.6: Configuration of the parallel back-propagation method based on a pre-dispersion mutual phase-conjugation system

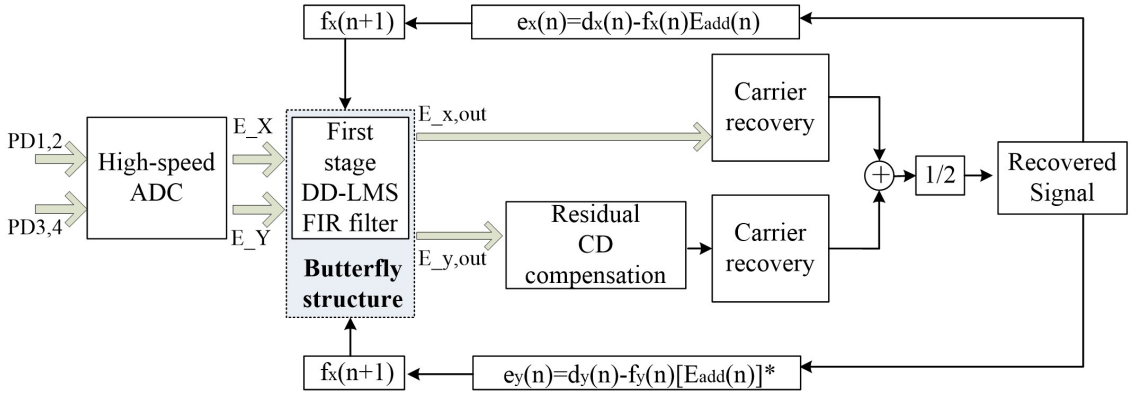

Figure 3.7: DSP algorithm for the parallel back-propagation method

The two streams of signals are transmitted simultaneously using polarization-division multiplexing (PDM). The receiver is shown in Fig. 3.7, which adds an extra block for residual CD mitigation because the unbalance between the MPC signals. The remains maintain same as the configuration of the MPC scheme.

3.2.3 Principle of the Parallel Back-Propagation

In Sec. 2.1.2, we introduce the conventional back-propagation method for fiber-nonlinearity mitigation. Although it provides satisfactory NL-mitigation effect, the

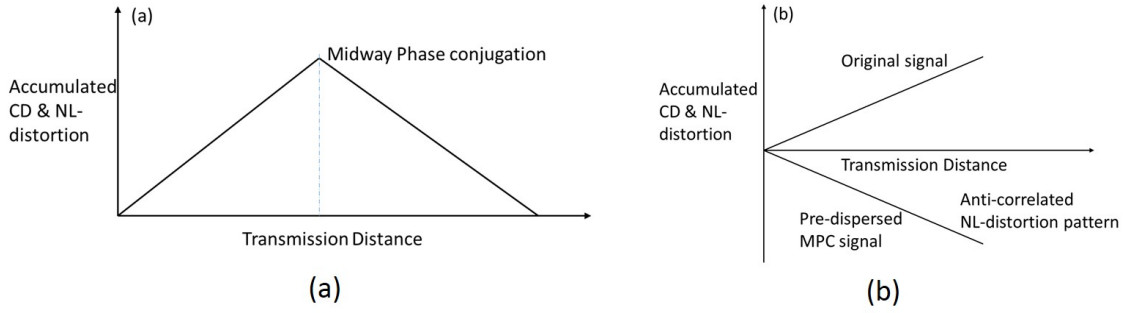

Figure 3.8: Schematic diagram of accumulation of the CD- and NL-distortion as a function of the transmission distance (a) in the midway phase-conjugation scheme and (b) in the pre-dispersed MPC scheme.

operation of phase-conjugation at the mid-point of the transmission link ultimately limits its application. In Sec. 2.2.3, the digital back-propagation method eliminates the physical phase conjugation at the midpoint, but computational complexity for the digital back-propagation is so large that the real-time operation of DSP is very difficult to achieve.

For the conventional back-propagation method, Fig. 3.8(a) illustrates the map of accumulate NL distortion along the fiber link. The fiber-nonlinearity is eliminated in a separate process, which limits its application. It is desirable to execute the back-propagation method in a parallel manner. It's realized by the *parallel back-propagation* method.

Fig. 3.8(b) shows the map of accumulated NL distortion of the PBP method along the fiber link. For the elucidation of the principle of the PBP scheme, we apply the perturbation method to Eq.r̃efeq:NLSEsp and Eq. 2.12. For clear analyses of NL distortion, we assume the system is free from noise and ignore the loss/gain distribution of the system.

The original signal E_{in} is transmitted on the x-polarization mode. The waveform of the received signal is conceptually composed of two parts as

$$E_{x-rx} = T[E_{in}] = D(E_{in}) + N(E_{in}) \tag{3.7}$$

where $D(E_{in})$ and $N(E_{in})$ represent linearly-dispersive term and nonlinearly-distorted term, respectively. T denotes the total transmission operator.

In the midway phase-conjugation system, the signal is phase-conjugated at the midpoint and re-transmitted through the same link. Then, the output signal returns to the phase-conjugated input signal in the back-propagation manner. This process is written as

$$E_{out-midway} = T[E^*_{x-in}] = T[D(E_{in})^* + N(E_{in})^*] = E^*_{in} \tag{3.8}$$

In the case of the PBP method shown in Fig. 3.8 (b), we cannot transmit $E^*_{x-rx} = D(E_in)^* + N(E_in)^*$, because such waveform is unknown at the transmitter. Instead, we can transmit $D(E_{in})^*$, which is pre-dispersed phase-conjugated signal. At the receiving end, the waveform of the received phase-conjugated signal is obtained as

$$E_{out-mpc} = T[D(E_{in})^*] \tag{3.9}$$

Then, Eq. 3.8 and 3.9 yield

$$E_{out-mpc} = E^*_{in} - T[N(E^*_{in})] \tag{3.10}$$

If we ignore the second-order nonlinear term, we have

$$E_{out-mpc} \simeq E^*_{in} - D[N(E^*_{in})] \tag{3.11}$$

Taking the operation of conjugation of the received signal in the phase-conjugated channel, Eq. 3.11 yields

$$E^*_{out-mpc} = E_{in} - D^{-1}[N(E_{in})] \tag{3.12}$$

The second term in Eq. 3.12 is generated because we transmit $D(E_in)^*$ instead of $D(E_in)^* + N(E_in)^*$ that realizes the perfect compensation in a back-propagation manner.

On the other hand, the original signal is transmitted on the orthogonal polarization

mode. After compensation for CD, the recovered signal becomes

$$E_{x-cd} = D^{-1}[D(E_{in}) + N(E_{in})] = E_{in} + D^{-1}[N(E_{in})] \tag{3.13}$$

Note that nonlinear terms in the two parallel channels are anti-correlated; therefore, adding these two signal together, we obtain

$$E_{add} = \frac{E_{x-cd} + E^*_{out-mpc}}{2} = E_{in} \tag{3.14}$$

The NL-distortion term is thus cancelled out with each other and the original signal is recovered.

The above analysis describes the NL distortion from SPM in the original signal and the phase-conjugated replica. In the PDM scheme, we need to take cross-phase modulation (XPM) between two polarization modes into account; however, this analysis is still applicable in such a case. This is because XPM-induced phase rotations on both signals are the same and XPM-induced distortions are anti-correlated at the output ports.

In the above analysis, the amount of dispersion DL, which is the total amount of dispersion of the link, is given to the phase-conjugated channel at the transmitter. However, if the amount of CD given to the phase-conjugated channel is larger than that given to the desired signal by DL, any amount of pre-dispersion can realize the same NL mitigation effect.

3.3 Conclusion

In this chapter, we present the principles of operations for our NL-mitigation method. The MPC scheme realizes lower signal power on each polarization mode to reduce the induced-SPM effect. It creates 3 dB intrinsic NL power tolerance improvement. For the PBP method, it generates the NL-mitigation pattern in a back-propagation manner parallel with the original signal transmitted. Therefore it effectively abates the fiber-nonlinearity and applicable for practical system implementation.

Chapter 4

Simulation results and discussion

In this chapter, we present the simulation results of the proposed methods for fiber-nonlinearity mitigation. The system setup is based on a 20-Gbit/s QPSK coherent system with 1,000-km-long dispersion-unmanaged link consisting of standard single-mode fibers (SMFs) only.

We designed simulations with various optical parameters to understand and verify the principle of the MPC and PBP method. The signal variance σ^2 is shown in comparison to the conventional scheme including the SP scheme and the DP scheme as a function of signal launched power, which illustrates the system performance of the proposed methods over conventional ones. Virtual BP link is designed in simulation to verify the generation of NL mitigation pattern in a back-propagation manner. Simulations for the 16-QAM modulation format are carried out for the verification of the general applicability of the MPC scheme.

In the designed simulation system, we verify the intrinsic 3-dB NL power tolerance improvement for the MPC scheme; for the PBP method, we find that the optimal signal power is improved by more than 7 dB. Both methods are applicable for practical system implementation independently of modulation format.

4.1 System setup

The simulation is based on a 20-Gbit/s QPSK coherent system through 1,000-km-long dispersion-unmanaged link with SMF only. The basic configuration is same as Figure 3.1. The system setup is as follows: the fiber is constructed by the fiber loop which is consisted of a 100-km standard single-mode fiber (SMF) and an EDFA with 4-dB noise figure. In some simulations, for the pure examination of the NL mitigation effect, the EDFA is set to be ASE-noise free. The EDFAs fully compensate for the span loss. The optical parameters of the fiber are 0.2 dB/km, 17 ps/nm/km, and 1.5 /W/km for the loss coefficient α, the CD parameter β_2, and the nonlinear coefficient γ, repectively. The laser linewidths for both transmitter and local oscillator (LO) are set to be 0 Hz, for the pure examination of the NL mitigation.

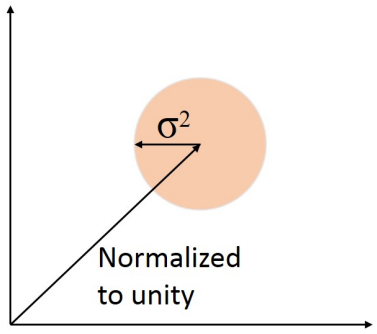

Figure 4.1: Concept illustration for the signal variance σ^2 which is normalized to unity in a QPSK system

For the evaluation of the signal quality, we calculate the variance σ^2 of the constellation-point distribution of the signals, where the carrier amplitude is normalized to unity. The illustration of the variance σ^2 is shown in the Figure 4.1. The calculation of the variance σ^2 follows the equation,

$$\sigma^2 = \frac{\sum(E(t) - \mu)^2}{N - 1} \tag{4.1}$$

where N is the number of symbol accounted, μ is the mathematical expectation of the received signal for each constellation point. The variance is calculated for each

constellation point and then averaged to generate the overall variance of the received signal.

The compensation ratio is calculated for the evaluation of SPM mitigation. It is defined as the between variances σ^2 of the signal E_{add} after the summation in Eq. 3.14 and the signal E_{x-cd} before the summation.

The NL power tolerance is the difference in the launched signal power giving a certain variance σ^2 between the SP and MPC schemes. It shows the improvement of the system robustness against NL distortion.

4.2 Discussion of the simulation results

4.2.1 Mutual Phase Conjugation scheme

First, we conducted the simulation of the MPC-QPSK system as a function of the launched signal power in comparison to the SP scheme and DP scheme to illustrate the 3-dBm NL power tolerance improvement. Fig. 4.2 shows the variance σ^2 of the MPC, SP, and DP scheme in red, blue, and black curve, respectively. We find that the NL tolerance of the MPC scheme is improved by 5 dB and 4 dB compared with SP and DP ones, respectively. There are 3 dB NL tolerance improvement stemmed from the signal power dissipation and the SNR enhancement described in Chapter 3. The extra compensation effect stems from mutual phase conjugation, because the similarity of the MPC signals in the initial stage induces similar NL distortion.

The signal variance σ^2 as a function of the transmission distance is shown in Fig. 4.3. The MPC scheme (red line) and the SP scheme (blue line) are transmitted at 0 dBm. The variance σ^2 is largely reduced in the MPC scheme, where the variance σ^2 of the MPC scheme at L km transmission distance is lower than that of the SP scheme at $\frac{L}{2}$ km transmission distance. It demonstrates the MPC scheme is more suitable for ultra-long distance transmission.

The MPC scheme is modulation format independent according to the analysis in Chapter 3. The simulation results of the 16-QAM MPC scheme and 64-QAM MPC scheme as a function of the launched signal power in comparison to the SP scheme is

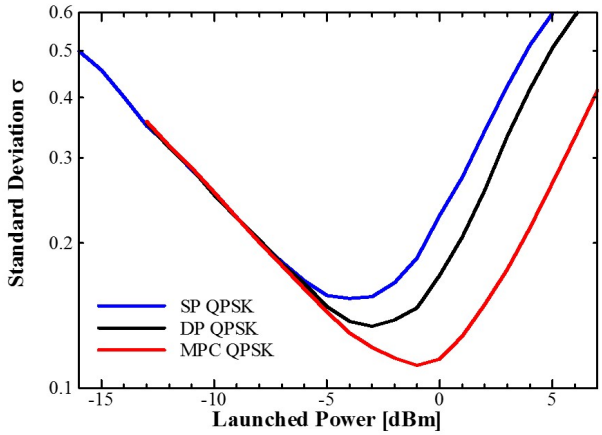

Figure 4.2: Simulation results of σ^2 in the 1,000-km 20-Gbit/s QPSK system calculated as a function of the lauched power for SP, DP and MPC schemes

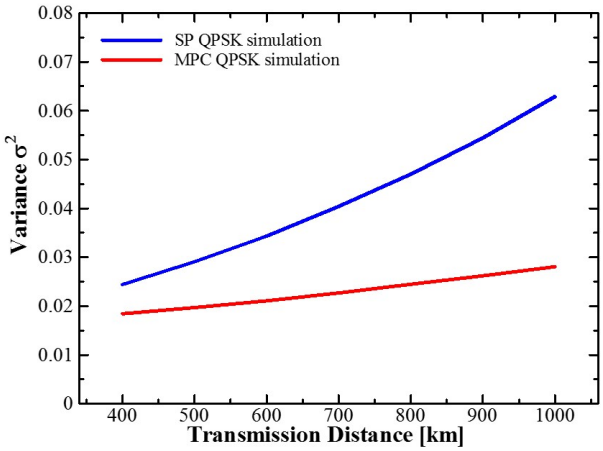

Figure 4.3: Simulation results of σ^2 in the 20-Gbit/s QPSK system as a function of the transmission distance for SP and MPC schemes. The launched power is 0 dBm

shown in Fig. 4.4(a) and (b), respectively. There is the 3-dBm intrinsic NL tolerance improvement although the optimal power value is different for each.

The above two figures illustrated show that the MPC scheme has 3-dB intrinsic NL tolerance improvement. In addition, there is extra SPM mitigation effect stemmed from the anti-correlation between two MPC waveforms in the initial spans. According to the simulation results, around 1-dB SPM mitigation effect is expected.

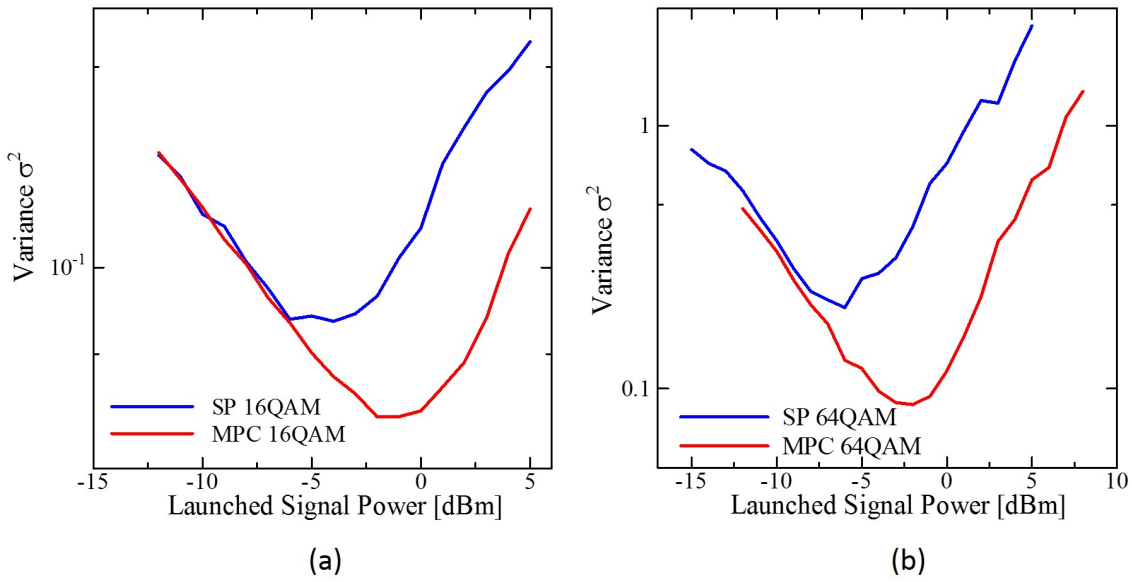

Figure 4.4: Simulation results of σ^2 in the 40-Gbit/s 16-QAM and 60-Gbit/s 64-QAM system as a function of the lauched power for SP, DP and MPC schemes

Because the anti-correlation between the two MPC signals is quickly disrupted by different CD pattern, the SPM mitigation effect of the MPC scheme from conjugation is limited. It is expected to increase the SPM mitigation effect from conjugation to further improve the NL mitigation effect using the PBP method.

4.2.2 Pre-dispersed Mutual Phase Conjugation scheme

The pre-dispersion MPC scheme can realize the *parallel back-propagation* method for highly effective SPM mitigation. We conducted extensive simulations to further examine the PBP method. The system configuration is the same as the one for the MPC scheme in Sec. 4.2.1, with additional electrical pre-dispersion in the transmitter, as described in Fig. 3.7. In the following part, we focus on the fiber-nonlinearity mitigation effect in QPSK systems.

Fig. 4.5 shows the compensation ratio of the virtual BP link (red) and the actual one (blue). In the virtual BP link, the link for the phase-conjugated y-polarization channel has the reversed loss coefficient of -0.2 dB/km as well as the reversed gain

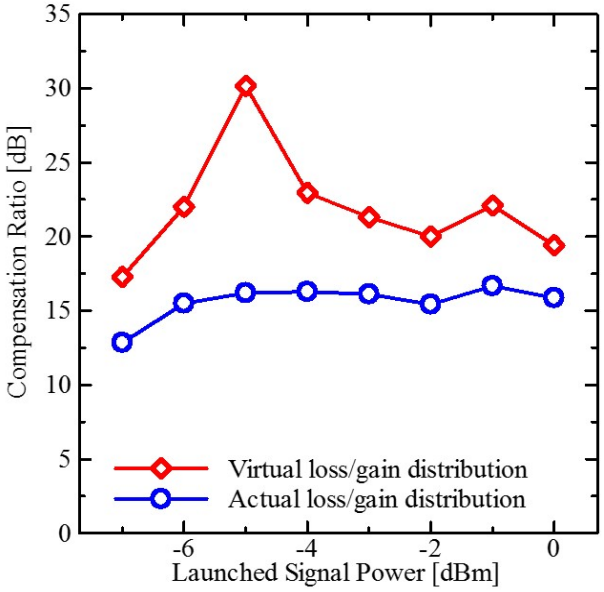

Figure 4.5: Simulation results of the compensation ratio in a 1,000-km 20-Gbit/s pre-dispersed MPC QPSK system as a function of the launched power.

of EDFAs, whereas the link for the x-polarization channel has the normal loss/gain distribution. On the other hand, the actual link has the normal loss/gain distribution for both of the channels. The ASE noise is neglected in both cases.

As shown in Fig. 4.5, in the signal power range from -7 dBm to 0 dBm, the compensation ratio of the virtual BP link is over 20 dB and around 5-dB better than that of the actual link. The enhancement of the compensation ratio owing to the virtual power map suitable for the phase conjugated channel proves that the generation of the NL mitigation pattern follows the mechanism similar to the back-propagation scheme. Note that the back-propagation method works ideally when the sign of the loss/gain coefficient is reversed [35].

Next, we calculate the compensation ratio in the real link as a function of the amount of pre-distortion. The launched power is fixed at 0 dBm and the ASE noise is neglected. The original signal is pre-dispersed with CD, whose amount ranges from $-2DL$ to $2DL$. The amount of CD given to the phase-conjugated replica is larger than that to the original signal by DL.

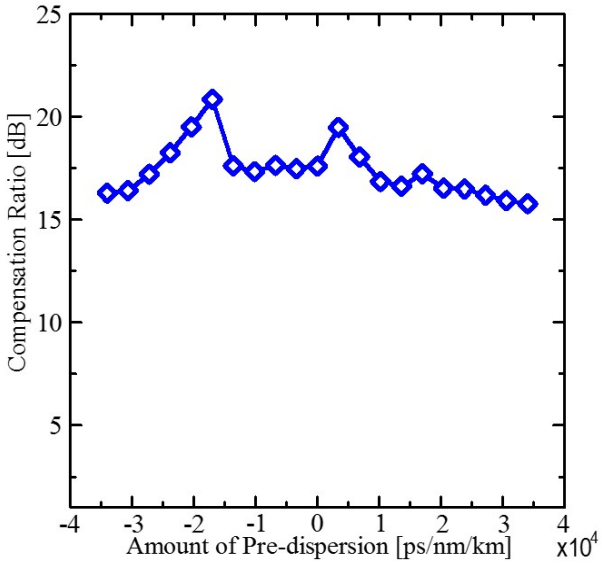

Figure 4.6: Simulation results of the compensation ratio in a 1,000-km 20-Gbit/s pre-dispersed MPC QPSK system as a function of the amount of pre-dispersion. The launched power is fixed at 0 dBm

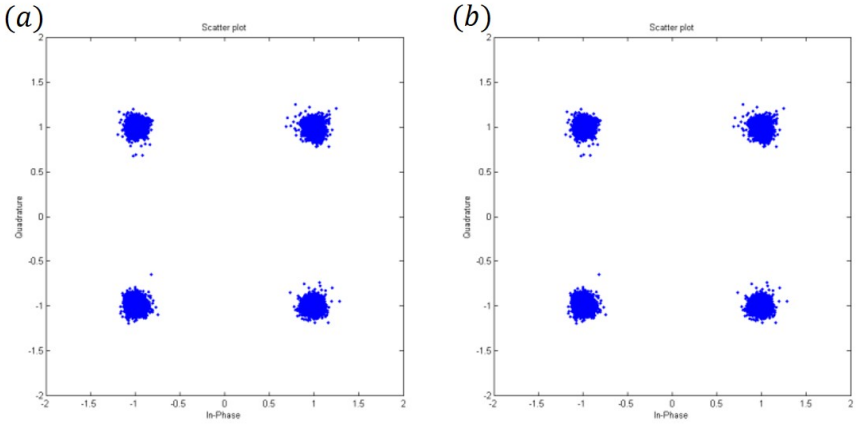

Figure 4.7: Signal constellation of received signal after NL mitigation in PBP method with different amount of pre-dispersion. The amount of pre-dispersion on original signal is (a) $-DL$, (b) DL. The signal power is fixed at 0 dBm

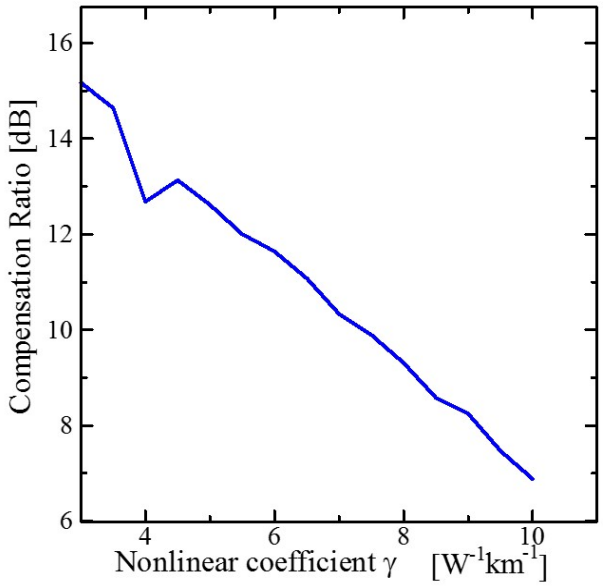

Figure 4.8: Simulation results of the compensation ratio in a 1,000-km 20-Gbit/s pre-dispersed MPC QPSK system as a function of the nonlinear coefficient. The launched power is fixed at 0 dBm

In Fig. 4.6, we find that the compensation ratio of the proposed method slightly fluctuates around 17 dB as the amount of the pre-dispersion on the MPC signals is varied in a wide range. It demonstrates that the amount of pre-dispersion on the MPC signals is not restricted by the dispersion map of the fiber link. Provided that the waveform of the original signal after propagation can be emulated using pre-dispersion, any amount of pre-dispersion is applicable to implement the PBP method for highly effective SPM mitigation effect. The corresponding constellations are shown in Fig. 4.7. In Fig. 4.7 from (a) to (b),the four MPC signals are pre-dispersed with $-DL$, and DL on the original signal, respectively. There is no significant difference among the constellations after the NL mitigation.

Fig. 4.8 is the compensation ratio as a function of the increasing NL coefficient γ in the simulated QPSK system. The ASE noise is neglected and the signal power is 0 dBm. The compensation ratio gradually decreases as the increase of the NL coefficient. It fits the analysis of the principle of the PBP method. As the increase of

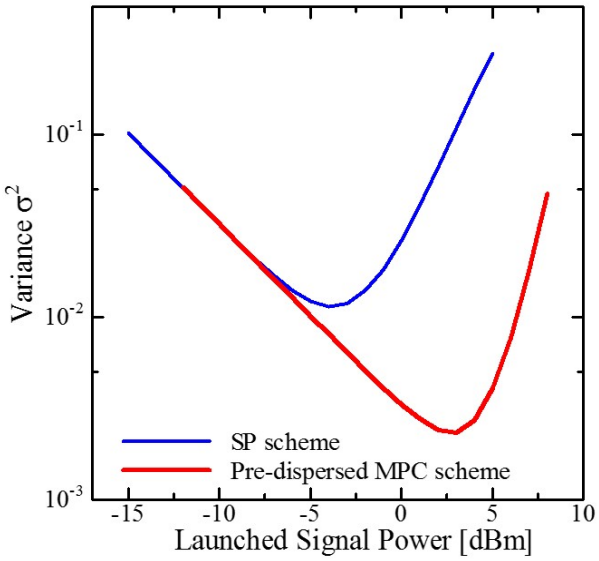

Figure 4.9: Simulation results of σ^2 in the 1,000-km 20-Gbit/s QPSK system as a function of the launched power for the SP (blue) and the pre-dispersed MPC scheme (red)

the NL term in the signal waveform, the interaction between the NL term becomes not negligible for SPM mitigation. A smaller fraction of NL term, namely a larger fraction of the CD term, is a desirable feature for fiber-nonlinearity mitigation system based on the PBP method.

Next, Fig. 4.9 shows variances σ^2 of the pre-dispersed MPC system (red curve) and the SP scheme (blue curve) as a function of the launched signal power. The amount of pre-dispersion on the MPC signals is set to $-DL/2$ because such a value induces the least SPM distortion on the transmitted signal [36]. In terms of the variance σ^2, the optimal power is increased to over 3 dBm in the proposed scheme, while that of the SP scheme is -4 dBm. The optimal signal power is improved by 7 dB. Compared with MPC scheme, there is 4 dB improvement, which enables system for a longer transmission distance. The NL tolerance power of the PBP method is over 10 dB when σ^2=0.02, achieving the 6-dB improvement in comparison with no pre-dispersion MPC scheme. It means the effective power range is up to 8 dBm for the QPSK system.

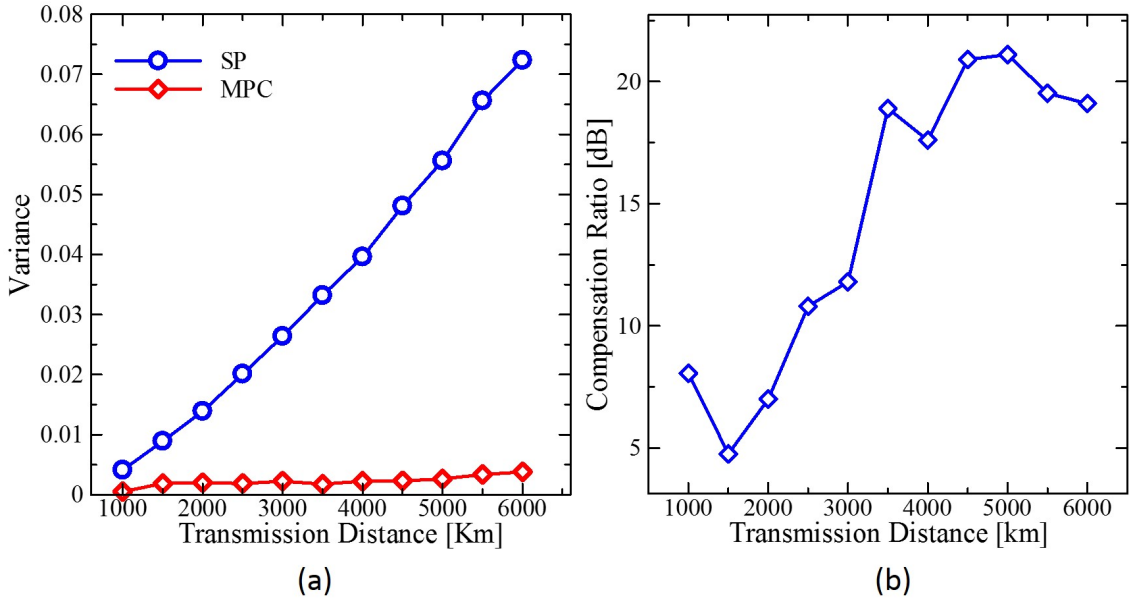

Figure 4.10: (a) Simulation results of σ^2 in the 20-Gbit/s QPSK system as a function of the transmission distance for the SP (blue) and the pre-dispersed MPC scheme (red); (b) Corresponding compensation ratio for the simulation result in (a). The signal power is 0 dBm.

As discussed in Chapter 3, the PBP method can mitigate nearly all the NL distortion using the PBP method provided that the signal power is within the effective power range. As for the QPSK system, the effective power range is up to 8 dBm. We conducted the simulation of the 0-dBn QPSK system using the PBP method in a 20-Gbit/s fiber system. The ASE noise is excluded.

In Fig. 4.10(a), the variance σ^2 as a function of the transmission distance is shown for the pre-disersion MPC scheme and SP scheme in red and blue curve, respectively. The signal power is 0 dBm. The variance σ^2 of the pre-dispersion MPC scheme maintains flat till 5,000 km, indicating the NL distortion is effectively eliminated using the PBP method. In comparison, there is a super-linear relationship between the variance σ^2 and the transmission distance for the SP scheme. The variance σ^2 of the pre-dispersed MPC scheme at 5,000 km is smaller than that of the SP scheme at 1,000 km.

After 5,000-km transmission, the variance σ^2 of the pre-dispersed MPC scheme slightly increases due to the accumulated NL term. The accumulated NL term deteriorates the emulation between the original signal at the receiver and the pre-dispersed MPC signal at the transmitter. The compensation ratio correspondingly decreases after 5,000 km, as shown in Figure 4.10(b). However, the compensation ratio has over 15 dB effect, indicating the PBP method is highly applicable for ultra-long fiber transmission system, even the compensation ratio slightly decreases as the increase of transmission distance.

4.3 Conclusion

In this chapter, we focused on the discussion of the simulations of the two proposed methods in a 1,000-km SMF-only 20-Gbit/s QPSK system.

We verified the effectiveness of the 3-dB intrinsic NL power tolerance improvement in comparison to the SP and DP schemes. This result is modulation independent. The 16-QAM system is conducted with the same improvement.

For the PBP method, we designed several simulations with different optical parameters to examine the principle of the SPM mitigation. We proved the NL mitigation pattern is generated in a similar mechanism of the back-propagation method.

Within the effective NL-mitigation power range, the NL distortion is nearly canceled out and the compensation ratio maintains at certain level within wide range of pre-dispersion. The optimal power of the PBP method is increased by 7 dB in comparison to the SP scheme and NL power tolerance power is over 10 dB when the variance $\sigma^2 = 0.02$, 6-dB improvement in comparison to the MPC scheme without pre-dispersion. The signal power and the accumulated NL term degrade the SPM mitigation effect, where the signal power has a more direct and significant impact on the mitigation effect. All the phenomenon observed in simulations fit the prediction in the analysis of Chapter 3.

Chapter 5

Experiment results and discussion

In this chapter, we conduct the experiments of the MPC method. The results demonstrate its effectiveness in fiber-nonlinearity alleviation. There is 3-dB intrinsic NL power tolerance improvement and extra SPM mitigation effect from the anti-correlation of conjugation. It is proved that the MPC method can extend the current transmission limitation over twice.

5.1 System setup

The experiment setup is illustrated in Figure 3.1. A distributed-feedback laser diode (DFB-LD) is used as the transmitter laser. The linewidth of the DFB laser is 100-kHz and the wavelength is centered in 1,552 nm. A differentially-encoded NRZ-QPSK signal was generated by a LiNbO3 optical IQM which was driven by a 10-GSymbol/s arbitrary waveform generator with $2^9 - 1$ PRBS. The AWG is used to generate both original and pre-dispersed signal with Nyquist pulse at the sample rate of 10-GSymbol. The pre-dispersed signal is generated by DSP and stored in AWG. For the DP scheme, PMD is executed by the split-delay-combine method; for the MPC scheme and the pre-dispersed MPC scheme, the MPC signals are generated by two IQMs and multiplexed into PMD by polarization beam combiner. The setup for the fiber link is the same as shown in the simulations. The actual loss per span is 23 dB including the splicing loss, which was compensated for by two cascaded EDFAs.

At the receiver side, the signals are detected by a homodyne phase- and polarization-diversity coherent receiver. A DFB-LD with same characters of one of the transmitter laser is used as the LO. The output power from the LO is 10 dBm. The asynchronously running ADCs then convert the optical signals into digital domain. The sampling rate of the ADCs is 50 GSymbol/s and the resolution is 8-bit. A set of data with 1-M samples is processed offline by DSP with fixed CD compensation; 255-tap FIR-filter-based equalization adapted by the DD-LMS algorithm for polarization demultiplexing and clock-phase recovery; and carrier-phase estimation. Note in the PBP method, the fixed CD compensation recovers the data with half the CD amount of the fiber link. Then the prepared training symbols of the dispersive signals are used for LMS algorithm. After the received signals are polarization demultiplexed, the residual CD is compensated for by another long-tap LMS FIR filter for each signal simultaneously with clock recovery and carrier recovery.

5.2 Discussion of the Experiment results

In this section, we present the experiment verification for our proposed two methods. All the experiments are based on the 1,000-km 20-Gbit/s all-SMF fiber coherent system. First, we verified the 3-dBm fundamental NL power tolerance improvement in the MPC scheme in comparison to the SP scheme and the DP scheme. Then we show the variance σ^2 as a function of the transmission distance of the MPC scheme in comparison to the SP schemes when the signal power is fixed at 0 dBm.

Figure 5.1 shows σ^2 as a function of the launched signal power for SP (blue), DP (black), and MPC (red) schemes without predispersion. In the NL region, the MPC scheme increases NL power tolerance by 4 dB and 3 dB against SP and DP schemes, respectively. Small disagreement from the simulation result (Fig. 4.2) may be due to imbalance of the two IQMs.

Then we conducted the experiment of the signal variance σ^2 as a function of transmission distance. The launched signal power was 0 dBm. Dashed blue and red curves in Fig. 5.2 show experimental results of σ^2 as a function of the transmission distance for SP and MPC schemes, respectively. The transmitted signal was received

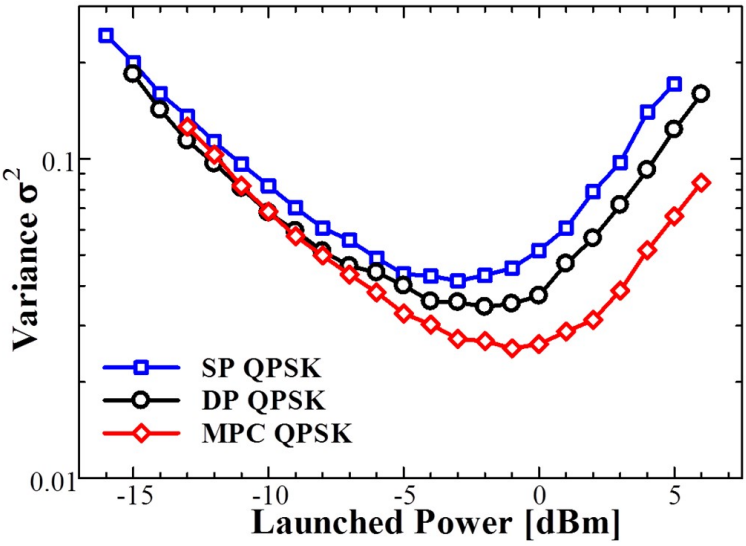

Figure 5.1: Experimental results of σ^2 in the 1,000-km 20-Gbit/s QPSK system measured as a function of the lauched power for SP, DP, and MPC schemes

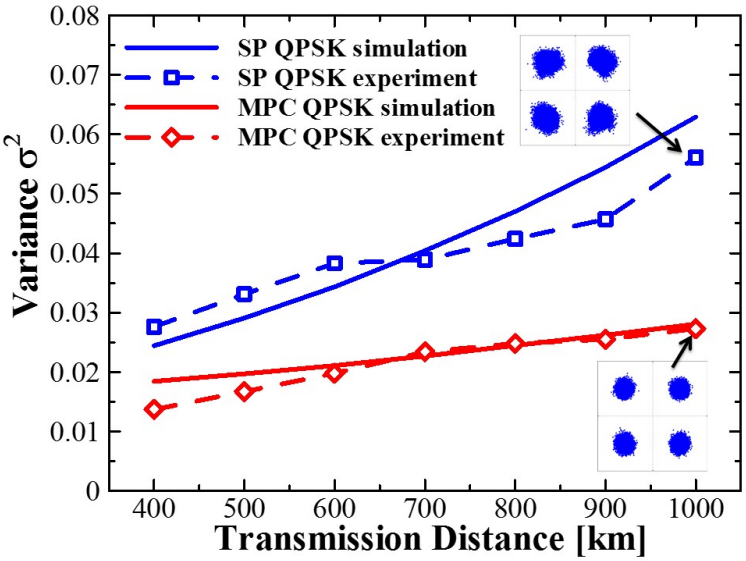

Figure 5.2: Simulation and experimental results of σ^2 in the 20-Gbit/s QPSK system as a function of the transmission distance for SP and MPC schemes. The launched power is 0 dBm.

every 100-km span until the total distance reached 1,000 km. The experiment results are in good agreement with those of simulations (solid curves), which confirms that our proposal can extend the limit of transmission distance over twice. Inset constellations are measured at 1,000 km for SP and MPC schemes, clearly showing the NL mitigation effect of the MPC scheme.

5.3 Conclusion

In this chapter, we present the experiment results for the MPC and PBP methods for fiber-nonlinearity mitigation. The MPC method demonstrates 3-dB intrinsic NL power tolerance improment in comparision to the SP and DP scheme at same bit rate with same modulation format. The transmission distance is demonstrated to be doubled in the MPC method.

Chapter 6

Conclusion

In this thesis, we study the principle of two novel fiber-nonlinearity mitigation methods: the mutual phase-conjugation method and the parallel back-propagation method.

In chapter 2, we reviewed the basic knowledge to understand the methods for fiber-nonlinearity mitigation, the mathematical model of lightwave propagation in single-mode fiber and the principle of digital coherent receiver. In addition, we explain two conventional methods for fiber-nonlinearity mitigation - the conventional back-propagation method and the digital back-propagation method.

In chapter 3, the principles of the mutual phase-conjugation method and the parallel back-propagation method are explained. We deduce the three factors contributing to the 3-dB NL power tolerance improvement in the MPC scheme. For the PBP method, we use mathematical deduction to demonstrate the generation of NL mitigation pattern in a back-propagation manner and its high performance for fiber-nonlinearity mitigation.

We conduct extensive simulations to demonstrate the effectiveness of the proposed methods for nonlinearity robust optical system. It's shown that there is 3-dB intrinsic NL power tolerance improvement from the MPC scheme and the optimal signal power is improved by 7 dB. The simulation results demonstrate the proposed methods are applicable for fiber-nonlinearity limited transmission system.

The experiments of the MPC scheme are conducted as well. The results are well fitted with the simulation results. Experiments related to the PBP method will be

finished in near future to demonstrate its effectiveness in fiber-nonlinearity mitigation.

In conclusion, we can mitigate the fiber-nonlinearity distortion with the proposed two methods effectively for real-time coherent optical system. Such methods release the limitation of the coherent optical communication system from fiber nonlinearity. It is expected to be widely used in ultra-long communication fiber system.

Appendix A

Publication list

Published works

Hongbo Lu, Yojiro Mori, Changyo Han, and Kazuro Kikuchi, "Novel polarization-diversity scheme based on mutual phase conjugation for fiber-nonlinearity mitigation in ultra-long coherent optical transmission systems, European Conference and Exhibition on Optical Communication (ECOC 2013), paper We3C.3, Sept. 22-26, 2013, London, UK.

Hongbo Lu, and Kazuro Kikuchi, "Pre-dispersed mutual phase-conjugation scheme for fiber-nonlinearity mitigation in coherent optical communication systems," Technical Committee on Optical Communication Systems (OCS), Aug. 22-23, 2013, Hokkaido, Japan

Yojiro Mori, Changyo Han, **Hongbo Lu**, and Kazuro Kikuchi, "Wavelength Demultiplexing of Nyquist WDM Signals under Large Frequency Offsets in Digital Coherent Receivers," European Conference and Exhibition on Optical Communication (ECOC 2013), paper Mo4C.6 , Sept. 22-26, 2013, London, UK.

In preparation

Hongbo Lu, and Kazuro Kikuchi, "Effective fiber nonlinearity mitigation in a practical manner using the parallel back-propagation method based onpre-dispersed mutual phase conjugation scheme," to be submitted to *Optics Express*

Bibliography

[1] Hadis Morkoç. Semiconductor lasers: Light amplification by stimulated emission of radiation. *Nitride Semiconductor Devices: Fundamentals and Applications*, pages 267–348.

[2] KC Kao and George A Hockham. Dielectric-fibre surface waveguides for optical frequencies. *Electrical Engineers, Proceedings of the Institution of*, 113(7):1151–1158, 1966.

[3] RG Smith and SD Personick. Receiver design for optical fiber communication systems. In *Semiconductor devices for optical communication*, pages 89–160. Springer, 1982.

[4] Takanori Okoshi. Recent advances in coherent optical fiber communication systems. *Lightwave Technology, Journal of*, 5(1):44–52, 1987.

[5] Hideki Ishio, Junichiro Minowa, and Kiyoshi Nosu. Review and status of wavelength-division-multiplexing technology and its application. *Lightwave Technology, Journal of*, 2(4):448–463, 1984.

[6] C Siva Ram Murthy and Mohan Gurusamy. *WDM optical networks: concepts, design, and algorithms*. Prentice Hall PTR Englewood Cliffs, 2002.

[7] Charles A. Brackett. Dense wavelength division multiplexing networks: Principles and applications. *Selected Areas in Communications, IEEE Journal on*, 8(6):948–964, 1990.

[8] RJ Mears, L Reekie, IM Jauncey, and DN Payne. Low-noise erbium-doped fibre amplifier operating at 1.54 μm. *Electronics Letters*, 23(19):1026–1028, 1987.

[9] Emmanuel Desurvire, Jay R Simpson, and PC Becker. High-gain erbium-doped traveling-wave fiber amplifier. *Optics Letters*, 12(11):888–890, 1987.

[10] Takanori Okoshi and Kazurō Kikuchi. *Coherent optical fiber communications*, volume 3. Springer, 1988.

[11] S. Tsukamoto, K. Katoh, and K. Kikuchi. Coherent demodulation of optical multilevel phase-shift-keying signals using homodyne detection and digital signal processing. *Photonics Technology Letters, IEEE*, 18(10):1131–1133, 2006.

[12] A. Sano, H. Masuda, T. Kobayashi, M. Fujiwara, K. Horikoshi, E. Yoshida, Y. Miyamoto, M. Matsui, M. Mizoguchi, H. Yamazaki, Y. Sakamaki, and H. Ishii. 69.1-tb/s (432 channels 171-gb/s) c- and extended l-band transmission over 240 km using pdm-16-qam modulation and digital coherent detection. In *Optical Fiber Communication (OFC), collocated National Fiber Optic Engineers Conference, 2010 Conference on (OFC/NFOEC)*, pages 1–3, 2010.

[13] Masato Yoshida, Hiroki Goto, Keisuke Kasai, and Masataka Nakazawa. 64 and 128 coherent qam optical transmission over 150 km using frequency-stabilized laser and heterodyne pll detection. *Opt. Express*, 16(2):829–840, 2008.

[14] Kazushi Toyoda, Yuki Koizumi, Tatsunori Omiya, Masato Yoshida, Toshihiko Hirooka, and Masataka Nakazawa. Marked performance improvement of 256 qam transmission using a digital back-propagation method. *Optics Express*, 20(18):19815–19821, 2012.

[15] D. Ly-Gagnon, S. Tsukamoto, K. Katoh, and K. Kikuchi. Coherent detection of optical quadrature phase-shift keying signals with carrier phase estimation. *Lightwave Technology, Journal of*, 24(1):12–21, 2006.

[16] Yojiro Mori, Chao Zhang, and Kazuro Kikuchi. Novel fir-filter configuration tolerant to fast phase fluctuations in digital coherent receivers for higher-order

qam signals. In *Optical Fiber Communication Conference*. Optical Society of America, 2012.

[17] Seb J Savory et al. Digital filters for coherent optical receivers. *Opt. Express*, 16(2):804–817, 2008.

[18] Seb J Savory. Digital coherent optical receivers: algorithms and subsystems. *Selected Topics in Quantum Electronics, IEEE Journal of*, 16(5):1164–1179, 2010.

[19] Robert W Tkach. Network traffic and system capacity: Scaling for the future. In *Optical Communication (ECOC), 2010 36th European Conference and Exhibition on*, pages 1–22. IEEE, 2010.

[20] Y Sun, AK Srivastava, S Banerjee, JW Sulhoff, R Pan, K Kantor, RM Jopson, and AR Chraplyvy. Error-free transmission of 32× 2.5 gbit/s dwdm channels over 125 km using cascaded in-line semiconductor optical amplifiers. *Electronics Letters*, 35(21):1863–1865, 1999.

[21] Y Miyamoto, A Hirano, K Yonenaga, A Sano, Hi Toba, K Murata, and O Mitomi. 320 gbit/s (8× 40 gbit/s) wdm transmission over 367 km with 120 km repeater spacing using carrier-suppressed return-to-zero format. *Electronics Letters*, 35(23):2041–2042, 1999.

[22] Yojiro Mori, Chao Zhang, Masatoshi Usui, Koji Igarashi, Kazuhiro Katoh, and Kazuro Kikuchi. 200-km transmission of 100-gbit/s 32-qam dual-polarization signals using a digital coherent receiver. In *Optical Communication, 2009. ECOC'09. 35th European Conference on*, pages 1–2. IEEE, 2009.

[23] Yuki Koizumi, Kazushi Toyoda, Tatsunori Omiya, Masato Yoshida, Toshihiko Hirooka, and Masataka Nakazawa. 512 qam transmission over 240 km using frequency-domain equalization in a digital coherent receiver. *Optics express*, 20(21):23383–23389, 2012.

[24] Benyuan Zhu, John M Fini, Man F Yan, Xiang Liu, S Chandrasekhar, Thierry F Taunay, Michael Fishteyn, Eric M Monberg, and Frank V Dimarcello. High-capacity space-division-multiplexed dwdm transmissions using multicore fiber. *Lightwave Technology, Journal of*, 30(4):486–492, 2012.

[25] Yiran Ma, Qi Yang, Yan Tang, Simin Chen, and William Shieh. 1-tb/s per channel coherent optical ofdm transmission with subwavelength bandwidth access. In *Optical Fiber Communication Conference*. Optical Society of America, 2009.

[26] R-J Essiambre, Gerhard Kramer, Peter J Winzer, Gerard J Foschini, and Bernhard Goebel. Capacity limits of optical fiber networks. *Lightwave Technology, Journal of*, 28(4):662–701, 2010.

[27] Govind P Agrawal. *Fiber-optic communication systems*, volume 222. John Wiley & Sons, 2010.

[28] A Carena, V Curri, G Bosco, P Poggiolini, and F Forghieri. Modeling of the impact of nonlinear propagation effects in uncompensated optical coherent transmission links. *Journal of Lightwave Technology*, 30(10):1524–1539, 2012.

[29] Chaloemphon Lorattanasane and Kazuro Kikuchi. Design theory of long-distance optical transmission systems using midway optical phase conjugation. *Lightwave Technology, Journal of*, 15(6):948–955, 1997.

[30] Kazuro Kikuchi. Coherent optical communication systems. *Optical Fiber Telecommunications VB: Systems and Networks, IP Kaminow*, pages 95–130, 2008.

[31] Abdul J Jerri. The shannon sampling theoremits various extensions and applications: A tutorial review. *Proceedings of the IEEE*, 65(11):1565–1596, 1977.

[32] Reinhold Noe. Pll-free synchronous qpsk polarization multiplex/diversity receiver concept with digital i&q baseband processing. *Photonics Technology Letters, IEEE*, 17(4):887–889, 2005.

[33] Ezra Ip and Joseph M Kahn. Feedforward carrier recovery for coherent optical communications. *Journal of Lightwave Technology*, 25(9):2675–2692, 2007.

[34] Y. Mori, K. Igarashi, K. Katoh, and K. Kikuchi. Decision-feedback carrier-phase estimation for digital coherent optical receivers. In *Opto-Electronics and Communications Conference, 2008 and the 2008 Australian Conference on Optical Fibre Technology. OECC/ACOFT 2008. Joint conference of the*, pages 1–2, 2008.

[35] Kazuro Kikuchi. Electronic post-compensation for nonlinear phase fluctuations in a 1000-km 20-gbit/s optical quadrature phase-shift keying transmission system using the digital coherent receiver. *Opt. Express*, 16(2):889–896, 2008.

[36] S. Fujisawa, D. Ogasahara, E.L.T. de Gabory, T. Ito, and K. Fukuchi. Mitigation of intra-channel nonlinear distortions based on papr reduction with cd pre-compensation in real-time 50gbps pm-qpsk transmission. In *Opto-Electronics and Communications Conference (OECC), 2012 17th*, pages 439–440, 2012.

Hongbo Lu

I certify that I have read this dissertation and that, in my opinion, it is fully adequate in scope and quality as a dissertation for the degree of Doctor of Philosophy.

(Kazuro Kikuchi) Principal Adviser

Approved for the University Committee on Graduate Studies
